# Sourcing and Long-Range Transport of Particulate Organic Matter in River Bedload: Rio Bermejo, Argentina

Sophia Dosch[1,2], Niels Hovius[1,2], Marisa Repasch[3], Joel Scheingross[4], Jens M. Turowski[1], Stefanie Tofelde[5], Oliver Rach[1], Dirk Sachse[1,6]

[1]GFZ German Research Centre for Geosciences, Potsdam, Germany
[2]Universität Potsdam, Institute of Geosciences, Potsdam, Germany
[3]University of Colorado Boulder, Institute of Arctic and Alpine Research, Boulder, CO, USA
[4]University of Nevada Reno, Department of Geological Sciences and Engineering, Nevada Geosciences, Reno, NV, USA
[5]Freie Universität Berlin, Institute of Geological Sciences, Berlin, Germany
[6]Humboldt Universität zu Berlin, Department of Geography, Berlin, Germany

*Correspondence to*: sophia.dosch@gfz-potsdam.de

## 1 Introduction

The burial of organic carbon (OC) in soils and sedimentary depocenters can remove carbon from the atmosphere over timescales of centuries to millennia (Hilton and West, 2020; Galy et al., 2015; Blair and Aller, 2012; Battin et al., 2009; Hayes et al., 1999; Stallard, 1998; France-Lanord and Derry, 1997; Berner, 1982). OC buried in sedimentary basins is mainly sourced from tectonically active environments, like mountainous areas where physical erosion mobilizes hillslope bedrock and soil, generating sediment (e.g., Galy et al., 2015; Blair and Aller, 2012; Stallard, 1998). Rivers play a key role as conduits in the carbon cycle, moving OC eroded from rock, soil and vegetation from terrestrial to marine carbon reservoirs if the transported carbon is buried in a sedimentary basin (e.g., Schlünz and Schneider, 2000). The long spatial and temporal scales of this transport allow for carbon transformation during transfer and intermittent storage (Blattmann et al., 2019; Galy et al., 2008), for instance in floodplains, estuaries, and coastal mud belts (Repasch et al., 2022; Scheingross et al., 2021; Canuel and Hardison, 2016; Aller, 1998).

It is usually assumed that once particulate organic matter (POM) from terrestrial sources has been transferred into rivers, it is transported with the fine suspended sediment (Kao et al., 2014). Estimates of POM flux, as opposed to dissolved OM, suggest that rivers deliver 110 – 230 MtC into the oceans annually (Galy et al., 2015). River bedload can comprise lithic fragments that contain fossil organic carbon (Smith et al., 2013b; Hage et al., 2020; Kao et al., 2014), a phase of particulate OC that might be oxidized and emit $CO_2$ during floodplain transit (Dellinger, 2023). A second organic bedload component consists of plant debris.

Particulate OM includes coarse plant material and can be abundant, ranging from 10 up to 80% of the total fluvial OC flux (Seo et al., 2008; West et al., 2011; Kao et al., 2014; Turowski et al., 2016). Hillslope mass wasting, overland flow, and flooding of riparian zones can mobilize leaf litter and woody debris into the fluvial routing system (Turowski et al., 2016; West et al., 2011; Wohl et al., 2009). Coarse POM can float at the river surface, where it is visible and accountable (e.g., Ruiz-Villanueva et al., 2019; West et al., 2011; Wohl et al., 2009), or it can move along the river bed where it is more difficult to observe and measure (e.g., Turowski et al., 2013). The physical, chemical, and biological breakdown of woody debris (Seo et al., 2008) resting in the landscape allows the material to become waterlogged within days or weeks (Hoover et al., 2010). This can increase the density of organic debris above the critical value of 1.0 g cm$^{-3}$ so that it will sink to the river bed (Turowski et al., 2016; Turowski et al., 2013). There, it can be transported with the bedload (e.g., Schwab et al., 2022; Hage et al., 2020; Lee et al., 2019; Turowski et al., 2016; Liu et al., 2016), and has been observed to comprise up to 75% of all coarse POM (Turowski et al., 2016).

Several studies describe fresh, coarse terrestrial organic debris transported to delta plains (Allen et al., 1979) and offshore (West et al., 2011) by turbidity currents (Hage et al., 2020; Liu et al., 2013; Tyson and Follows, 2000). When capped by muddy siliciclastic sediments, terrestrially sourced, coarse POM is protected from fast degradation (Hage et al., 2020; Lee et al., 2019; McArthur et al., 2016; Sparkes et al., 2015), leading to preservation rates of up to 70% (Hage et al., 2022; Kao et al., 2014). Coarse woody debris and litter fragments have been described in aged deep marine fan deposits (Lee et al., 2019) and to represent up to 12% of the mass in exhumed turbidites layers (Turowski et al., 2016; Tyson and Follows, 2000). Taken together, these observations suggest that transport of terrestrial POM in river bedload may be a relevant pathway in the global carbon cycle (Hage et al., 2020; Lee et al., 2019; Kao et al., 2014), both during source to sink transit and in depocenters.

However, organic debris at the river bed is difficult to observe and quantify due to logistical difficulties in sampling and highly variable transport rates (Turowski et al., 2013). The occurrence, recruitment, sources and fate of $POM_{Bed}$ during transport has only been addressed for a few headwater streams (Turowski et al., 2016; Turowski et al., 2013; Bunte et al., 2016; Iroumé et al., 2020; Fogel and Lininger, 2023), and even less for lowland systems (Hage et al., 2022; Schwab et al., 2022). The paucity of work on the origin of $POM_{Bed}$, and its endurance in long-range fluvial transport after erosion, makes it difficult to build a mechanistic model to predict bedload OC fluxes and quantify their role in the terrestrial OC cycle.

In this study, we evaluate the role of organic bedload in the OC cycle of a large lowland river, the Rio Bermejo in northwest Argentina. This river is a major tributary to the Rio Paraguay, draining a section of the eastern central Andes across an 800 km wide foreland without overwhelming human intervention (Repasch, 2023). The lowland portion of the Rio Bermejo has no major tributaries or distributaries over a flow distance of almost 1300 km, ruling out sediment mixing complexities inherent to dendritic drainage networks. We address three questions designed to understand the role of $POM_{Bed}$ in the terrestrial carbon cycle: 1) Is POM transported with bedload in the lowland Rio Bermejo? 2) If so, what are the source areas and mechanisms for $POM_{Bed}$ recruitment? 3) Does $POM_{Bed}$ survive long-range transport without transformation through the Rio Bermejo? To answer these questions, we collected organic-rich material traveling at the river bed, analyzed the geochemical composition of the collected organic-rich material and tracked compositional changes with increasing distance downstream from the headwaters.

## 2 Study Area, Sampling Methods and Analyses

### 2.1 Study area

The Rio Bermejo, catchment area of 120,283 km$^2$, drains the northern-western Argentinian Andes before crossing the Gran Chaco alluvial plain and joining the Rio Paraguay (Fig. 1a). The Rio Bermejo headwaters extend to the eastern limit of the arid Puna Plateau, at an elevation of ~4 km. Headwater streams drain high-altitude dry grasslands, ultimately merging to form the upper Rio Bermejo in the north and the Rio San Francisco (a major headwater tributary of the Rio Bermejo) in the south (Fig. 1). In the southern headwaters, mean annual rainfall is around 1000 mm yr$^{-1}$ and dense Yungas forests cover deeply weathered foothills. In the northern headwaters, the hinterland comprises the Eastern Cordillera and the Sub-Andean zone with highly variable rainfall up to 1400 mm yr$^{-1}$ and Yungas montane forest (Fig. 1c). Steep relief and intense precipitation in these northern headwaters result in high sediment yields to the Rio Bermejo.

At the Andean Mountain front, the upper Rio Bermejo and the Rio San Francisco merge to form the lowland Rio Bermejo, a sand bed river crossing the foreland basin. Just after the headwater confluence, the lowland Bermejo exhibits a braided morphology, with river width varying from 1-3 km. 175 km downstream of the confluence, the river transitions into a meandering channel, with migration rates from 40-80 m yr$^{-1}$. The channel width narrows to 170 m in the most downstream parts, towards the confluence with the Rio Paraguay (Repasch, 2023; Repasch et al., 2020; Sambrook Smith et al., 2016). River depth ranges between 4 to 10 meters at high flow with channel depth increasing downstream (Sambrook Smith et al., 2016). The daily water discharge averages 432 m$^3$ s$^{-1}$, however, the wet season discharge of the austral summer accounts for ~75% of the annual

95  flow, with daily discharges up to 2,000 m³ s⁻¹ (Golombek et al., 2021; Sambrook Smith et al., 2016). Grain size analyses show downstream fining of the suspended river load (Repasch et al., 2020) from medium sand, on average 280 μm in the headwaters, to very fine sand to silty sand, on average 90 μm in the downstream part of the river (Sambrook Smith et al., 2016; McGlue et al., 2016). The Rio Bermejo delivers ~80 Mt yr⁻¹ of suspended sediment to the Rio Paraguay. Suspended sediment input from the Andean headwaters at the Bermejo-San

100  Francisco confluence is significantly higher, ~103 Mt yr⁻¹, suggesting net deposition during foreland transit (Repasch et al., 2020). The Rio San Francisco contributes ~14% to the total suspended sediment load of the Rio Bermejo mainstem, whereas, the northern headwaters contribute ~86% (Repasch et al., 2020), likely reflecting the south to north gradient in precipitation, vegetation, and erosion rate.
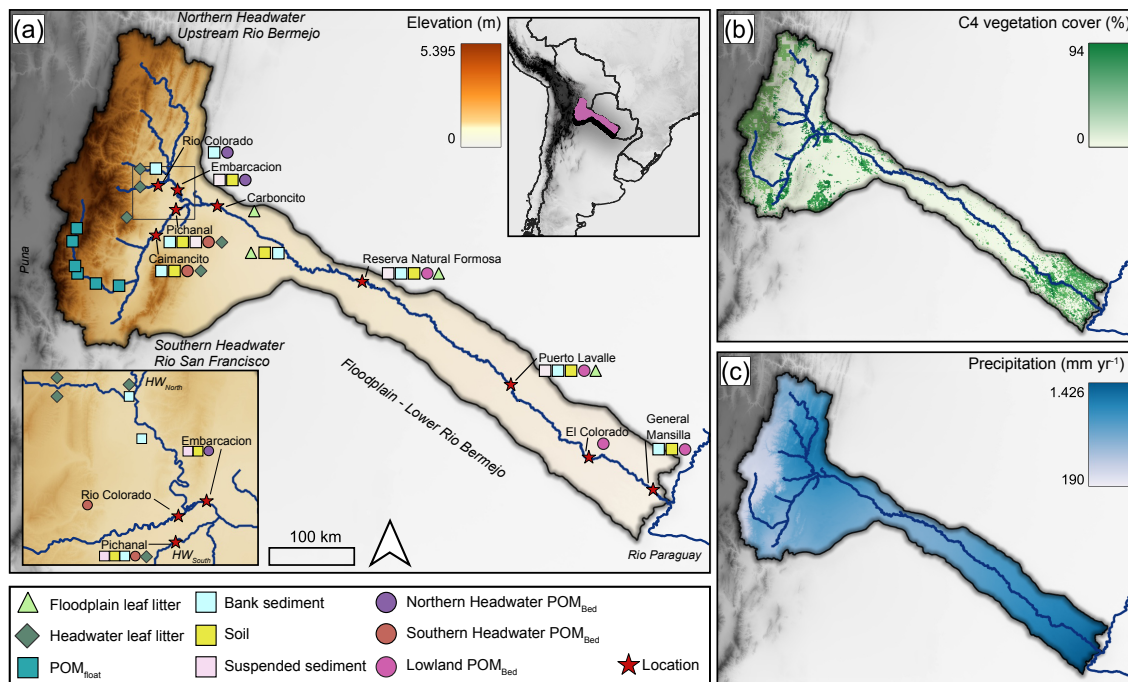
**Figure 1:** Catchment overview of the Rio Bermejo mainstem and main headwater tributaries (a) Topographic map (ASTGTM, Spacesystems and Team, 2019) with sample types indicated at each sampling location. Top right: catchment location in Argentina. Bottom left: zoomed view of the tributary confluence at the mountain front. (b) C4 vegetation cover, as a percentage of total C3 and C4 vegetation cover (Powell et al., 2012). (c) Average annual precipitation rate (Hijmans et al., 2005).

Our work is focused on the Rio Bermejo downstream of the east Andean Mountain front, from the

105  confluence of the Rio Bermejo and the Rio San Francisco at 304 m. asl. to the Rio Bermejo-Rio Paraguay confluence at 50 m asl.. The linear distance between these points is ~700 km, while the river has a channel length of ~1300 km due to its high sinuosity. Over this distance, no significant tributaries join the Rio Bermejo, making it an ideal setting for our source to sink study of organic bed material.

110  **2.2 Sampling**

During sampling campaigns in 2013, 2015, 2017, 2019 and 2020, we collected headwater and lowland floodplain leaf litter, coarse floating particulate organic matter (POMfloat, >1 cm diameter), soils from dry paleochannels, river bank sediments, suspended sediment, and bedload material in the Rio Bermejo catchment

(Table 1, Fig. 1a). Sampling of bedload was curtailed by pandemic travel restrictions coming into force during fieldwork in March 2020.

The sampling sites at Rio Colorado and Embarcacion are located within the northern headwaters (HW$_{North}$), and Caimancito and Pichanal are sampling sites in the southern headwaters (HW$_{South}$) along the Rio San Francisco (Fig. 1a). We sampled the Rio Bermejo main stem at five separate locations between the upstream most location at Carboncito (14 km linear distance downstream of the mountain front confluence), and the downstream most site at General Mansilla (660 km linear distance downstream of the mountain front confluence) (Fig. 1, Table 1).

**Table 1:** Overview of the bedload sampling sites, location, number of samples and type of sampling

| Location ID | Location name | Latitude | Longitude | Bermejo catchment | Distance from mountain front (km) | Year | n | Sample type |
|---|---|---|---|---|---|---|---|---|
| AR20SD01 | Caimancito HW$_{South-2}$ | -23.7109 | -64.5366 | Southern Headwater *Rio San Francisco* | -22 | 2020 | 2 | Transect |
| AR20SD05 | Rio Colorado HW$_{North-2}$ | -23.2962 | -64.2191 | Northern Headwater *Upper Rio Bermejo* | -16 | 2020 | 4 | Transect |
| AR20SD02 | Embarcacion HW$_{North-1}$ | -23.2479 | -64.1375 | Northern Headwater *Upper Rio Bermejo* | -10 | 2020 | 4 | Transect |
| AR20SD03 | Pichanal HW$_{South-1}$ | -23.3559 | -64.1827 | Southern Headwater *Rio San Francisco* | -15 | 2020 | 13 | Transect |
| AR17MR30 | Pichanal | -23.3559 | -64.1827 | Southern Headwater *Rio San Francisco* | -15 | 2017 | 1 | Single point |
| AR17MR17 | Reserva Natural Formosa | -24.3058 | -61.8345 | Downstream *Rio Bermejo* | 249 | 2017 | 1 | Single point |
| AR20SD15 | Puerto Lavalle LL$_{-1}$ | -25.6654 | 60.1282 | Downstream *Rio Bermejo* | 481 | 2020 | 12 | Transect |
| AR20SD18 | El Colorado LL$_{-2}$ | -26.3444 | -59.3614 | Downstream *Rio Bermejo* | 584 | 2020 | 8 | Transect |
| AR17MR57 | El Colorado | -26.3444 | -59.3614 | Downstream *Rio Bermejo* | 584 | 2017 | 1 | Single point |
| AR17MR05 | General Mansilla | -26.6613 | -58.6314 | Downstream *Rio Bermejo* | 660 | 2017 | 1 | Single point |

### 2.2.1 Bedload sampling: POM$_{Bed}$

In March 2020, we collected bedload material from cross-channel transects (Fig. 2a) at four locations upstream of the Bermejo-San Francisco confluence. At HW$_{South}$, we sampled the Rio San Francisco at Pichanal (HW$_{South-1}$, n=13) and at Caimancito (HW$_{South-2}$, n=2). At HW$_{North}$, we sampled the upper Rio Bermejo at Embarcacion (HW$_{North-1}$, n=10), and the Rio Colorado tributary (HW$_{North-2}$, n=4) (Fig. 1). Downstream of the confluence, we sampled the lowland Rio Bermejo mainstem at Puerto Lavalle (LL$_{-1}$, n=12), 481 linear km (X km streamwise) downstream of the confluence, and at El Colorado (LL$_{-2}$, n=8), 583 linear km (X km streamwise) downstream of the confluence (Table 1).

We collected bedload samples with a Helley-Smith bedload sampler with a 100 μm mesh and a 8×8 cm square opening (KC Denmark A/S, 2023). We ballasted the sampler with 12 kg weight to enable sinking to the river bed and attached a rope on both ends of the sampler. We deployed the device systematically from bridges across the Rio Bermejo and Rio San Francisco, where possible multiple times along a transect (Fig. 2a). We lowered the sampler to touch gently on the riverbed for 60 seconds and then manually pulled it up as quickly as possible, usually in less than 15 seconds, to minimize capture of material from shallower water column depths. We additionally collected bedload samples at one location per sampling site for a longer period, usually around 5 minutes, to attempt the collection of a sufficient amount of organic bedload material for compositional analysis. The wet samples were stored in air-tight Whirl-Pak plastic bags and transferred to Potsdam, Germany within two

weeks. The samples were freeze dried and dry-sieved over a stainless-steel sieve with 1 mm mesh size. Of the 49 bedload samples collected in 2020, 30 yielded no or less than one gram of macroscopic organic material ($POM_{Bed}$), many from downstream sampling sites. For selected samples with abundant organic debris in both fractions, we processed and analyzed the organic bedload material following the protocol described in Sect. 3.2 for both the >1 mm and <1 mm size fractions separately. We found no significant differences between the two size fractions, and therefore analyzed the remaining bedload samples as bulk.

In earlier sampling campaigns, we collected individual bedload samples throughout the catchment (Table 1): In March 2017, we collected single-point bedload samples with a self-built device at one headwater site, $HW_{South}$ (Pichanal, Rio San Francisco), and three mainstem Rio Bermejo sites: Reserva Natural Formosa, El Colorado, General Mansilla (Fig. 1a). In November 2019, six bedload samples were collected with a bedload grab that did not yield enough OM to permit compound-specific stable isotope measurements or significant amounts of $POM_{Bed}$. The sampling in these earlier campaigns was performed for the qualitative assessment of $POM_{Bed}$ occurrence and corresponding data were not used to quantitatively estimate $POM_{Bed}$.

For our purpose, we define $POM_{Bed}$ as organic material that is entrained within the clastic bedload, transported as separate layer on top of the clastic bedload, or that moves close to the river bed. It is likely that the $POM_{Bed}$ material is transported in a more extensive layer above the bed (Repasch et al., 2022; Schwab et al., 2022) also including saltating trajectories (Einstein et al., 1940; Turowski et al., 2010). The maximum particle size of the bedload samples was likely limited by the funnel opening width of 8 cm, as has been demonstrated for clastic bedload (Bunte et al., 2008), and our sample collection was restricted to the material transported within 8 cm above the bed. Our sample sizes may reflect these limitations of bedload sampling rather than a physical phenomenon. We assume, however, that these potential sampling biases do not affect the composition of the sample material.

### 2.2.2 Leaf litter and $POM_{float}$

During campaigns in 2015, 2019, and 2020, we collected 17 leaf litter samples within the floodplain ranging in elevation from 138 to 271 m asl., and 11 leaf litter samples from $HW_{North}$ and $HW_{South}$ upstream of the Rio Bermejo – Rio San Francisco confluence, between 317 – 854 m asl (Fig. 1). We typically collected ~20 g of leaf litter, the samples were air dried in the field and stored in paper bags upon arrival at the laboratory in Potsdam, Germany. There, the samples were oven-dried at 40°C for up to three days, and stored until further analysis.

We collected seven samples of floating, coarse particulate organic matter ($POM_{float}$, > 1 mm) along the Rio San Francisco (between 313 m asl and 2458 m asl) during the high flow season in March 2013 (Fig. 1a). These samples were collected with a net with mesh size 1 mm, held into the river water from the river banks until a sufficient amount of organic material was accumulated, and contained organic and inorganic debris ranging from 1 mm to 10 cm. The sample material was stored in plastics bags and freeze-dried upon return to the laboratory. The dry sample masses ranged from 5 to 40 g.

### 2.2.3 Soil, bank and suspended sediment

During campaigns in 2019 and 2020, we collected 15 sediment and 24 soil samples from the river banks and from a paleochannel on the Rio Bermejo megafan, at elevations of ~60 to 390 m asl. We used a rinsed, stainless-steel shovel to collect material from 0 to 20 cm below surface. The samples were stored in paper bags

and air dried in the field. Upon returning to the laboratory, we oven-dried all samples at 40°C for up to three days, and transferred them into brown glass bottles before analysis. We also include data on suspended sediment particulate organic carbon abundance and composition in the Rio Bermejo from previous studies (Repasch et al., 2021; 2022). Briefly, 48 samples were collected from several locations spanning $HW_{South}$, $HW_{North}$, and the lowland Rio Bermejo (Fig. 1a).
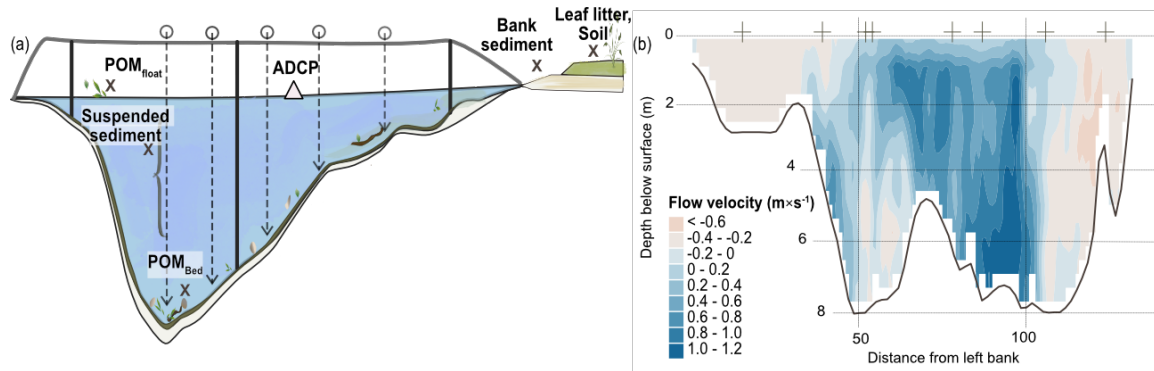
**Figure 2:** (a) Schematic channel cross section with transect sampling points (arrows), sample types used in this study, and indicated sample locations. (b) Cross-channel velocity profile using Acoustic Doppler Current Profiler at the $LL_{-2}$ station, crosses indicating each transect sampling point at the station. Bridge pillars were at 30, 75 and 125 m, measurements were taken ~5 m downstream of the bridge.

## 3 Methods: Analysis and data treatment

### 3.1 Near-bed flow velocity and channel depths

During the 2020 campaign, we determined the flow velocity and channel depth at the sampling locations $HW_{North-1}$ and $HW_{South-1}$ near the confluence, and downstream at $LL_{-1}$ and $LL_{-2}$. Surveys were conducted from bridges using an Acoustic Doppler Current Profiler (ADCP; Sontek RiverSurveyor RS-M9). The ADCP was mounted on a floating board and towed by a rope from the bridges. We applied strong tension to the rope in an effort to prevent the ADCP from being submerged under the bridge. Where possible and necessary, the ADCP float was guided by a person in the water. The raw ADCP data was processed using the SonTek RiverSurveyor Live Software (Version 4.1). After quality assessment in the SonTek Software, we further processed the data files using the velocity mapping toolbox (v.4.09) (Parsons et al., 2013) to calculate smoothed mean cross sections with the river flow velocity determined at horizontal and vertical grid node spacing of 1 m and 0.5 m, respectively. We extracted the river depth and flow velocity at each bedload sampling point by overlaying our GPS data points with these cross sections. To approximate the bedload transport velocity, we multiplied the depth-averaged streamwise flow velocity from the ADCP velocity profiles by 0.7 (Chatanantavet et al., 2013).

The ADCP-estimated near-bed flow velocity ranged between -0.17-1.19 m s$^{-1}$ and was on average 0.5 m s$^{-1}$±0.4 m s$^{-1}$ for the ensemble of sampling sites (n=4). We attribute occasional negative flow velocities to local flow patterns on large river bedforms (Allen, 1968), and assign no general significance to them (Fig. 2b). River depths measured during the wet season varied between 8.1-8.5 m at $HW_{South-1}$ and $HW_{North-1}$, 1.9-9.9 m at $LL_{-1}$, and 2.4-8.4 m at $LL_{-2}$ (Table S01). Due to the interrupted campaign in March 2020, these values do not cover the braided section of the river in the upper part of the east Andean foreland.

The high flow velocities and water depths of the Rio Bermejo made clean sampling of river bedload difficult, and the composition of some samples may have been affected by admixture of suspended load during sampler recovery. This is most likely to occur in the sediment-laden upper reaches of the Rio Bermejo and at downstream sites where bridge pillars cause additional turbulence.

## 3.2 Organic-geochemical analysis and raw results

To fingerprint source areas of the OM collected in this study, we use biomarker proxies, specifically long-chain $n$-alkanes, recalcitrant organic molecules that are often preserved in sediments (e.g., Thomas et al., 2021; Cranwell, 1972). Long-chain $n$-alkanes stable carbon and hydrogen isotopes incorporate local environmental conditions at formation, and therefore can help to track the source areas of POM in river sediment (e.g., Hemingway et al., 2016; Hoffmann et al., 2016; Bouchez et al., 2014; Ponton et al., 2014; Galy et al., 2011; Sachse et al., 2004).

We extracted $n$-alkanes from all samples and measured the compound-specific stable hydrogen and carbon isotope ratios. Soil, bank sediment, suspended sediment and $POM_{Bed}$, samples were ground with a mortar and pestle and lipid compounds were extracted with 9:1 methanol:dichloromethane, using a ThermoFisher Dionex Accelerated Solvent Extraction system (ASE 350). The non-polar $n$-alkane fraction was separated from the total lipid extract over silica gel columns with glass fiber filters at the base and top (pore size 60 Å, 230–400 mesh particle size) by automated solid-phase extraction (SPE) with a Gilson ASPEC GX-271 and $n$-hexane as solvent, following procedures described by (Rach et al., 2020). $n$-alkanes were extracted manually from leaf litter and $POM_{float}$ by immersing between 0.2 and 10.0 g of the dried samples in a 9:1 methanol:dichloromethane mixture and placing them into an ultrasonic bath at 40°C for 20 to 40 minutes. The $n$-alkanes were separated from the total liquid extract by solid phase extraction (SPE) over a silica gel-equipped 6 mL glass column (Macherey-Nagel, Düren, Germany) using $n$-hexane as solvent (Rach et al., 2020). The solid parts stayed behind and samples were rinsed properly with 9:1 DCM/MeOH. The lipid containing solvents were dried in the TurboVap and the lipids transferred to a smaller vial in approximately 1.5 ml 9:1 DCM/MeOH. The solvents of the TLE were evaporated again with N2 gas and the samples dissolved in 1.5 ml n-hexane. To quantify $n$-alkane concentrations per sample, we added an internal standard, 5α-androstane (10 $\mu$g), and measured the samples in an Agilent gas chromatograph (GC 7890-A) with a flame ionization detector (FID) and a coupled single quadrupole mass spectrometer (MS 5975-C).

We quantified the abundances of $n$-alkane homologues relative to the internal standard using the FID chromatograms. We calculated the average chain length ($ACL_{25-33}$) of the most abundant $n$-alkanes with chain lengths between 25 and 33 as:

$$ACL_{25-33} = \frac{\Sigma(C_n * n)}{\Sigma C_n} \tag{1}$$

$n$ is the number of carbon atoms of each $n$-alkane, and $C_n$ is the concentration of each $n$-alkane with $n$ carbon atoms. The subscripts on $ACL_{25-33}$ refer to the chain length range analyzed.

We determined the carbon preference index ($CPI_{25-33}$) after (Bray and Evans, 1961) for $n$-alkanes with 25 to 33 carbon atoms, using

$$CPI_{25-33} = \frac{1}{2} * \left( \frac{\Sigma C_{25-33odd}}{\Sigma C_{24-32even}} + \frac{\Sigma C_{25-33odd}}{\Sigma C_{26-34even}} \right) \tag{2}$$

245 $\Sigma C_{25\text{-}33\text{odd}}$ is the sum of the concentration of odd-chained *n*-alkanes with chain lengths between 25-33, concentration, $\Sigma C_{24\text{-}32\text{even}}$ the sum of the concentration of even-chained *n*-alkanes with chain lengths between 24-34, and so forth.

To measure compound-specific hydrogen and carbon isotope ratios of the *n*-alkanes (expressed as $\delta^2H$, $\delta^{13}C$

250 values), we used a Trace GC 1310 (ThermoFisher Scientific) connected to a Delta V plus Isotope Ratio Mass Spectrometer (IRMS) (ThermoFisher Scientific), following the procedures described by Rach et al. (2020). *n*-alkane $\delta^2H$ and $\delta^{13}C$ values were measured in duplicates. For each sample run, we measured the *n*-alkane standard-mix A6 (with n-alkane chain lengths ranging from *n*C16-*n*C30) with known $\delta^2H$ values obtained from A. Schimmelmann (Indiana University), for correction and transfer to the VSMOW scale. The H3+ factor from the

255 $^2H$ measurements was 5.9±0.8 mV. The standard deviation for $\delta^2H$ of the standard measurements was 2.3±0.7‰, and the mean standard deviation for the samples was 1.1±1.6‰. The mean standard deviation for $^{13}C$
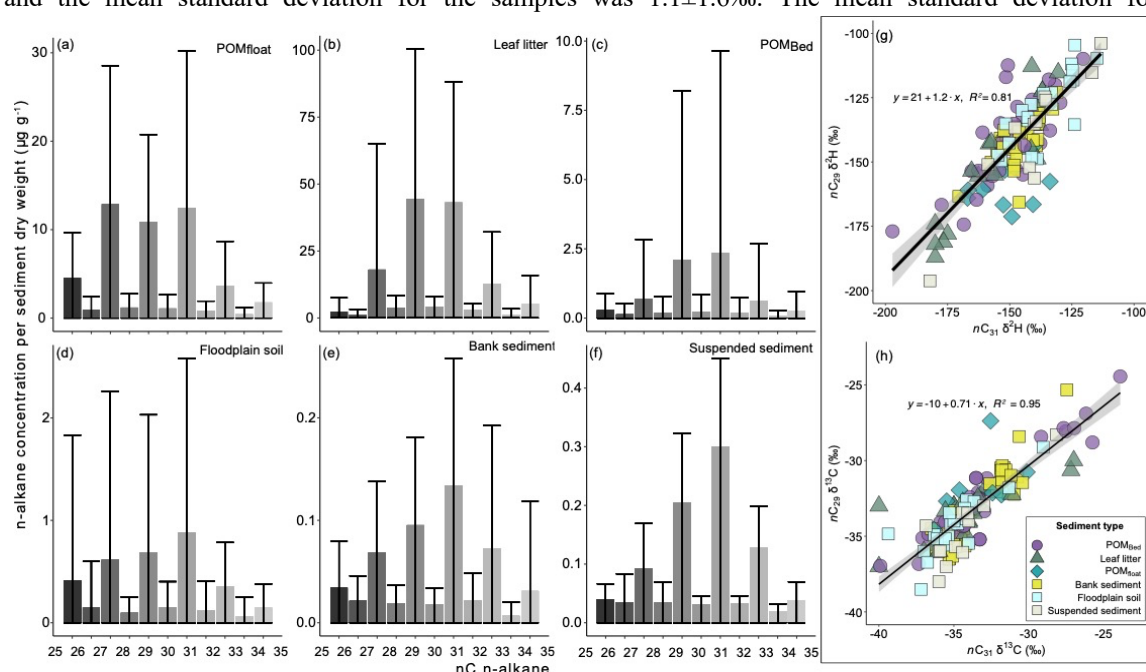
**Figure 3:** Left panel (a-f): Average and standard deviation (bars and whiskers) of the long-chain n-alkane distribution (*n*C$_{25}$-*n*C$_{35}$) as concentration per sediment dry weight (µg g$^{-1}$) of (a) POM$_{float}$, (b) leaf litter, (c) POM$_{Bed}$, (d) floodplain soil, (e) bank sediment and (f) suspended sediment. Note the different y-scale ranges. Right panel (g, h): *n*C$_{29}$ versus *n*C$_{31}$ *n*-alkane (g) $\delta^2H$ and (h) $\delta^{13}C$ values of all OM sample types, and linear regression equation and R$^2$ values.

measurements of the standard measurements was 0.11±0.06‰, and the mean standard deviation for the samples was 0.15±0.23‰.

### 3.2.1 Organic-geochemical raw results

260

We calculated the ACL$_{25\text{-}33}$ index for 201 samples collected in the Rio Bermejo catchment, including POM$_{Bed}$, leaf litter, POM$_{float}$, soil, sediment deposits, and river suspended sediment. *n*-alkanes with chain-lengths ranging from *n*C$_{25}$ – *n*C$_{35}$ had the highest abundance across all samples (Fig. 3, a-f). The main components were *n*C$_{31}$, *n*C$_{29}$ and *n*C$_{27}$, followed by *n*C$_{33}$ and *n*C$_{25}$, while even carbon numbered *n*-alkanes were minor components

265 in all samples. Leaf litter, POM$_{Bed}$ and soil samples had similar concentrations of *n*C$_{29}$ and *n*C$_{31}$. In river bank and suspended sediment samples, *n*C$_{31}$ was the dominant *n*-alkane, whereas *n*C$_{27}$ was the main component of the POM$_{float}$ samples. We measured the $\delta^2H$ and $\delta^{13}C$ values for the dominant chain lengths, *n*C$_{29}$ and *n*C$_{31}$. Because

these $n$-alkanes showed a significant correlation for $\delta^{13}C$ ($R^2 = 0.95$, $p < 0.01$) and $\delta^2H$ values ($R^2 = 0.81$, $p < 0.01$, Fig. 3g, h), we will focus on the $nC_{29}$ values.

For a subset of ten $POM_{Bed}$ samples with abundant organic debris in both the >1 mm and <1 mm fractions ($HW_{South-1}$, $HW_{South-2}$, $HW_{North-1}$, $HW_{North-2}$, $LL_{-1}$, $LL_{-2}$), we analyzed the $n$-alkane composition of $POM_{Bed}$ in both size fractions. In most of these samples, the two size fractions had distinct $ACL_{25-33}$, $CPI_{25-33}$, $nC_{29}$ $\delta^2H$ and $nC_{29}$ $\delta^{13}C$ values (Fig. S01). However, no discernible pattern emerged in these differences. For this reason, and because size-specific biomarker analyses were not possible for smaller sample amounts, we decided to work with $n$-alkane data from the bulk sample material. For samples analyzed as two separate fractions, we determined values for the bulk sample material as the weighted average of the two fractions. These values are dominated by the fraction <1 mm, which had the greater mass in all cases. In the following, we will refer to the results of analyses of the total particulate organic carbon of the sampled bedload material in the full-size range as $POM_{Bed}$.

### 3.3 Data analysis

All data analyses were performed using R 4.1.2 GUI 1.77 High Sierra build (8007). We report the range of the values as average ± standard deviation, and the number of samples. We used the Kolmogorov-Smirnov-Test to account for the non-normal distribution of our data and the Mann-Whitney U test to test for significant differences between independent sample groups. We used linear regression and associated $R^2$ values to test for significant trends in our data. Significance levels are reported at the 95% confidence interval (p-value < 0.05).

### 4. $POM_{Bed}$ presence, source and ability to survive long distance transport

We aim to answer questions regarding the source, transport, and survival of $POM_{Bed}$ in the Rio Bermejo. First, we want to observe when and where $POM_{Bed}$ is in active fluvial transport and how $POM_{Bed}$ composition varies throughout the catchment. We then investigate the sources of $POM_{Bed}$ by determining the elevation and climate of the OM source using $n$-alkane $\delta^2H$ value, assess the biological variability of $POM_{Bed}$ sources using $\delta^{13}C$ values combined with $ACL_{25-33}$, and estimate $POM_{Bed}$ maturity using $CPI_{25-33}$. Finally, we apply a mixing model using these geochemical data to define distinct $POM_{Bed}$ sources. Collectively, this approach allows us to evaluate the survival and fate of $POM_{Bed}$ during long-range fluvial transport in the Rio Bermejo.

### 4.1 Is there transport of $POM_{Bed}$ in the lowland Rio Bermejo and what is its geochemical composition?
### 4.1.1 Bedload mass and material composition

The mass of bedload samples comprising organic and clastic particles was up to an order of magnitude greater at the headwater sites than at the downstream sites for the same sampling procedure. Sampling at $HW_{South-1}$ and $HW_{North-1}$ yielded totals of 560 g min$^{-1}$ (n = 13), and 259 g min$^{-1}$ (n = 10), respectively, while at $LL_{-1}$ we collected a total of 51 g min$^{-1}$ (n = 12), and at $LL_{-2}$ 77.1 g min$^{-1}$ (n = 8), respectively (Fig. 4d, Table S01). The mass of dry $POM_{Bed}$ in individual bedload samples varied from 0g to ~20g, without clear spatial patterns. The mass of organic bedload scaled loosely with the amount of clastic sediment collected (Fig. 4d), but there was no correlation of the collected material and near-bed velocities. The material collected in $POM_{Bed}$ samples ranged from fragile, intact leaves and twigs to robust wood fragments with frayed edges and organo-clastic aggregates in the size range from <1 mm to ~10 cm, often mixed with fine organic debris <1 mm (Fig. 4). The organo-clastic

aggregates were easily dissociated during sieving, separating into fine sand and silt, and apparently degraded OM particles ranging from <1 mm to >1 cm (Fig. 4).

Chemical maturity of an OM sample can be expressed with the $CPI_{25-33}$, where lower values indicate a higher sample maturity due to chemical alterations of the OM. The strong predominance of odd-over-even *n*-alkane chain lengths in $POM_{Bed}$ ($CPI_{25-33}$ average: 7.4±3.0, n = 39, Fig. 5), and the $ACL_{25-33}$ averaging 29.6±0.9 (range: 27.4-31.6, n =39, Fig. 5) throughout the catchment indicate relatively fresh or little-degraded vascular plant material in the Rio Bermejo bedload (Eglinton and Hamilton, 1967; Bray and Evans, 1961). The occurrence of low $CPI_{25-33}$ <1 values in our dataset may be due to the occasional presence of burnt OM, such as charcoal particles, in the river bedload. While it is difficult to evaluate the volumetric contribution of this low $CPI_{25-33}$ material, it is negligible relative to other $POM_{Bed}$ sources.

The $POM_{Bed}$ fraction <1 mm consisted of mixed organic debris and clastic sediment and the coarser fraction >1 mm was composed predominantly of organic debris. Only at location $HW_{South-1}$ the Rio San Francisco carried substantial amounts of pebbles in the fraction >1 mm, while organo-clastic aggregates were more abundant at downstream sites. The geochemical analysis also revealed substantial differences in the size fractions >1 mm and <1 mm $POM_{Bed}$ in nearly all samples with sufficient mass for an articulated analysis (Fig. S01). The
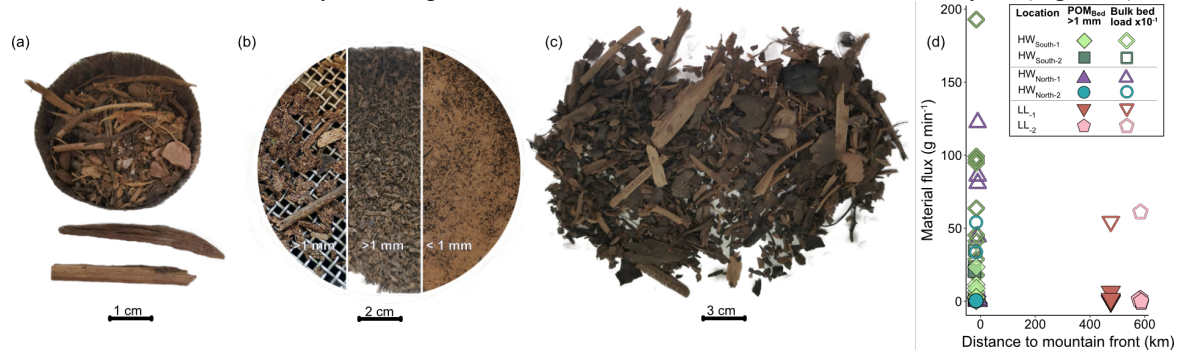
**Figure 4:** Examples of captured $POM_{Bed}$ as (a) bulk fraction from the Rio San Francisco at $HW_{South-1}$, (b) Rio Bermejo at $LL_{-1}$, in particle size separates: >1 mm, aggregated (left) and dissociated (middle), and <1 mm mixed with clastic material, (c) bulk at the Rio Bermejo at $HW_{North-1}$, and (d) sampled bulk bed material (empty symbols) and $POM_{Bed}$ > 1 mm (filled symbols) per sampling point at all sampling locations. Note the unequal x-axis breaks, and that $POM_{Bed}$ > 1 mm is shown in in g min$^{-1}$, and bulk bed material in in g min$^{-1}$ x10$^{-1}$, to account for the mass difference of the samples.

compositional differences between size fractions, as measured in our limited sample set, lack any discernible systematics, suggesting that variable sourcing affects both size fractions. Variable proportions of woody debris versus leaf fragments, biogeochemical quality, and size distribution indicate significant variability in the sourcing of materials of different sizes at each sampling location of $POM_{Bed}$ even within a single site (Fig. S01b, f). This implies that OM fragments in the Rio Bermejo bedload have diverse histories and indicates incomplete mixing both across the channel and along the length of the river, possibly due to highly active channel migration in some parts of the foreland. We did not measure the particle size distributions within individual samples, to have sufficient sampling material for geochemical analysis, but we detected a clear reduction in grain size between headwater and downstream locations (Fig. 4).

Geochemically, the similarity of $POM_{float}$, leaf litter, soils, sediments, and $POM_{Bed}$ suggests that all of the former can be sources of the sampled $POM_{Bed}$ and no major transformations have occurred during fluvial transit (Fig. 5). Leaf litter and soil inputs from hillslope and riparian areas have potential to be important sources adding to the $POM_{Bed}$ from the headwaters, yet, the sampled soils contained little to no coarse POM, suggesting that

eroded soil is more likely to become river suspended sediment than POM$_{Bed}$. Therefore, POM$_{float}$ and leaf litter are likely more important contributors to the POM$_{Bed}$ load. Another presumable POM$_{Bed}$ source is abundant woody debris in the catchment; however, this material contains insufficient *n*-alkanes to perform the same analysis. POM$_{Bed}$ CPI$_{25-33}$ values (average: 7.4±3.0, n = 39) were not significantly different from leaf litter (7.4 ±4.0, range:1.0-19.8, n = 28) and river bank sediments (6.5±3.7, range: 0.3-13.7, n = 18). However, on average POM$_{Bed}$ CPI$_{25-33}$ values were significantly higher than in soils (5.9±3.6, range: 0.2-16.3, n = 29) and suspended sediments (5.5±1.0, range: 1.1-7.8; n = 41), indicating a lower maturity of POM$_{Bed}$. CPI$_{25-33}$ values of POM$_{float}$ were substantially higher than values in all sediment samples (15.0±8, range: 2.4-27.9, n = 6), indicating it was, on average, less degraded than other sampled OM.

Before we analyze the details of POM$_{Bed}$ sourcing, we discuss the mechanisms of POM$_{Bed}$ recruitment.
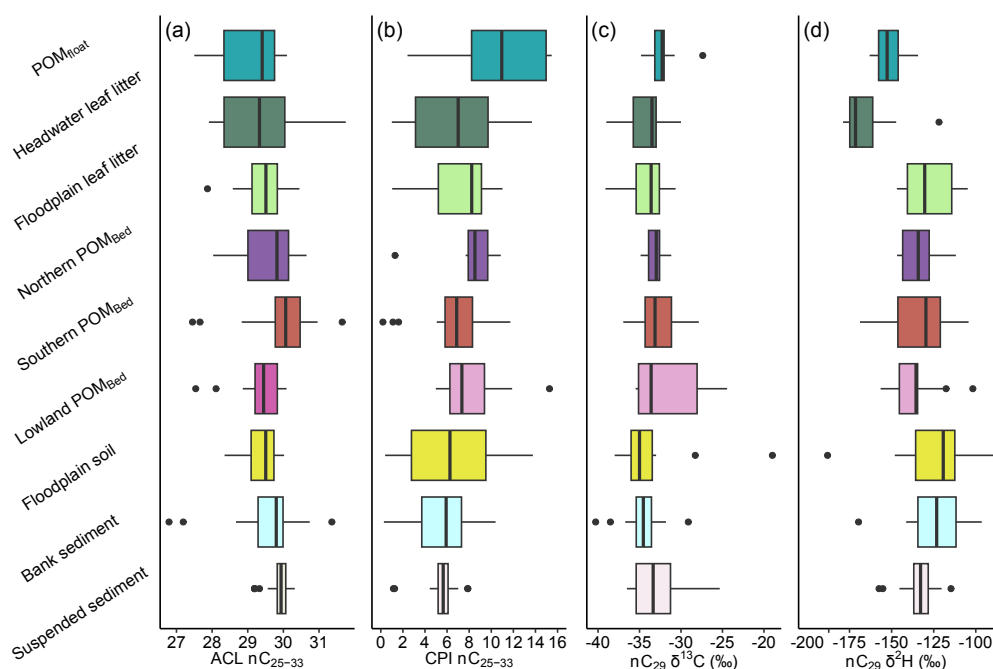
**Figure 5:** Summary of (a) ACL$_{25-33}$, (b) CPI$_{25-33}$, (c) $n$C$_{29}$ δ$^{13}$C and (d) $n$C$_{29}$ δ$^2$H values of POM$_{float}$, headwater and floodplain leaf litter; POM$_{Bed}$ from the northern headwater, southern headwater and downstream floodplain; floodplain soil, bank sediment, and suspended sediment. Boxplot width shows the interquartile range, black line the median, whiskers minimum and maximum range of the data without outliers. Black dots indicate outliers with 0.75 Quantile + 1.5 x interquartile range and 0.25 Quantile - 1.5 x interquartile range, respectively.

### 4.1.2 Mechanisms of recruitment and transport of POM$_{Bed}$

POM$_{Bed}$ is ubiquitous in the bedload of the Rio Bermejo throughout the catchment during the high flow season (Dec-Apr), when the South American Monsoon drives intense precipitation events throughout the study area. In contrast, we did not recover significant amounts of POM$_{Bed}$ during the low flow season. The high variability in δ$^2$H values from POM$_{Bed}$ sampled in 2017 and 2020, and the lack of significant amounts of POM$_{Bed}$ during the dry season of 2019 suggest that the processes of recruitment and transport occur quickly, possibly on (sub)seasonal timescales. The significantly higher CPI$_{25-33}$ values of POM$_{float}$ (Fig. 5b) suggest that the degradation of organic debris occurs after it becomes waterlogged. However, aerobic decomposition seems unlikely during active bedload transport, due to the high turbidity and depth of the river water. Instead, fresh plant debris is likely stored intermittently on hillslopes, floodplains or in-stream during the low flow season (May-Nov), where it can be degraded to various extents and waterlogged. With onset of the strong precipitation and high-water levels, it is

mobilized by overland flow, hillslope mass wasting, or lateral channel erosion, (e.g., Wohl et al., 2019; Turowski et al., 2016; Smith et al., 2013b; Hilton et al., 2012; Hilton et al., 2008; Selva et al., 2007), and subsequently transported as $POM_{Bed}$ (Turowski et al., 2016) during the high flow season.

In the headwaters, the erosive potential during the high flow season may exceed the production of organic debris in the riparian corridor on a seasonal timescale, limiting the supply of organic debris to the channel (Hilton et al., 2012; Yager et al., 2012; Garcia et al., 1999), and, consequently, the recruitment of $POM_{Bed}$. In this case, $POM_{Bed}$ export may peak early in the high flow season and diminish over the course of the season as the supply of organic debris is progressively reduced with each subsequent rain storm and $POM_{Bed}$ travels steadily downstream, similar to findings of seasonal sourcing of suspended OC at the Rio Bermejo (Golombek et al., 2021).

In the lowland floodplain, $POM_{Bed}$ recruitment is also highly seasonal, but the mechanism of recruitment differs from the steep headwater portion of the catchment (Wohl et al., 2019). Lateral channel migration eats into the floodplain forests, mobilizing large volumes of sediment, soil, leaf litter, and standing biomass with each bank failure. Bank erosion is most active at the peak of high flow season, providing a source of fresh OM to $POM_{Bed}$, and contributing to the poorly mixed nature of $POM_{Bed}$. However, poorly mixed samples could be expected at high rates of lateral migration from the upstream confluence to ca. 400 km downstream, but enhanced mixing seems more likely in segments with less active migration in the furthest downstream reach of the Rio Bermejo. Our results do not indicate enhanced mixing downstream, possibly because of the quick transport timescales, compared to the production and recruitment of $POM_{Bed}$.

Both upland and lowland lateral erosion processes are markedly reduced during the low flow season, aligning with our observations of ubiquitous $POM_{Bed}$ transport in Dec-Apr and negligible $POM_{Bed}$ transport in May-Nov.

**4.2 What are the source areas for recruitment of $POM_{Bed}$ and does it survive long-range transport?**

In the previous section, we concluded that $POM_{Bed}$ is a heterogenous mixture of OM from various sources in the catchment. In this section, we first aim to determine the stable carbon and hydrogen isotope composition of potential source materials. Subsequently, we apply a model to define the mixing space, using source and $POM_{Bed}$ geochemical compositions. In this, our aim is to determine the sources of Rio Bermejo $POM_{Bed}$, in order to determine its transformation and fate during long-range transit.

**4.2.1 Biomarker stable isotope insights into $POM_{Bed}$ source areas**

The stable carbon and hydrogen isotope composition of long-chain *n*-alkanes is used in paleoclimate research to reconstruct continental paleo vegetation (e.g., Sachse et al., 2012; Huang et al., 2007; Schefuss et al., 2005; Freeman and Colarusso, 2001), or to deduce environmental conditions and potential sources of OM (e.g., Hemingway et al., 2016; Bouchez et al., 2014; Galy et al., 2011; Sachse et al., 2004). Building off these approaches, we use $ACL_{25-33}$, $nC_{29}$ $\delta^{13}C$ and $\delta^2H$ isotope compositions (Fig. 5) to determine the source areas of $POM_{Bed}$ in the Rio Bermejo catchment.

395 *n*-alkane $\delta^{13}C$ values in plants are controlled by the plant metabolism type, with C3 plants around -37 - -27‰ and

C4 plants around -22 - -10‰ (e.g., Garcin et al., 2014; Huang et al., 2007; Freeman and Colarusso, 2001; Collister

et al., 1994). Rio Bermejo POM$_{Bed}$ $n$C$_{29}$ $\delta^{13}C$ values averaged -32.4±2.9 (range: -36.9 - -24.4‰, n = 35, Fig. 5d),

reflecting an overall C3-dominated plant input (Garcin et al., 2014). Silva et al. (2011) identified a shift towards

C3 vegetation in our study area in the last ~3000 years. This imposes an age cap for the organic bedload material,

400 below which our observation of predominance of fresh to degraded organic material can be accommodated.
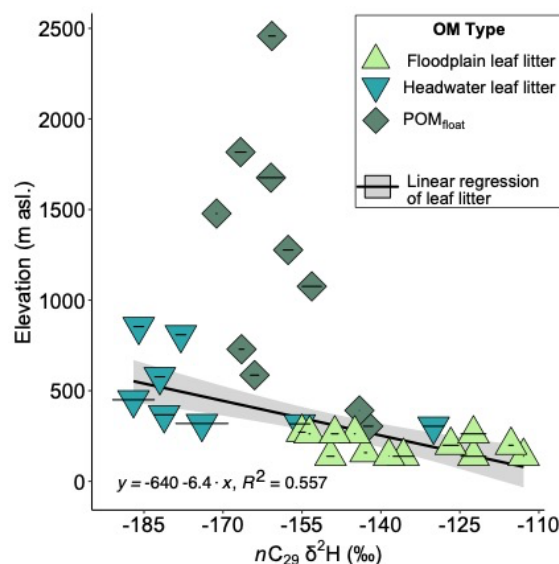
**Figure 6:** Sampling elevation and $n$C$_{29}$ $\delta^2H$ values of floodplain and headwater leaf litter, and POM$_{float}$. Colors represent the organic matter type; symbols represent the catchment source area. The linear regression was done using floodplain and headwater leaf litter data. Linear regression of POM$_{float}$ samples is not shown and was not significant. Measurement uncertainty is plotted inside the symbol.

There were no distinct differences between the POM$_{Bed}$ $\delta^{13}C$ values and those for catchment soil (-34.5±2.2‰,

range: -40.2 - -29.1‰, n = 22), deposited sediment (-33.7±4.5‰, range: -38.0- -18.9‰, n = 16), and floodplain

leaf litter (-33.9±2.2‰, range: -39.1 - -30.6‰, n = 15), signaling that all these reservoirs are dominated by C3

405 inputs (Fig. 5a, c). However, local findings of more positive $\delta^{13}C$ values, and higher ACL$_{25-33}$ (Fig. 7) suggest C4

plant contributions to POM$_{Bed}$, possibly from maize cultivation in the HW$_{South}$ catchment area (Powell et al., 2012),

and to a lesser extent in the lowland reach near LL$_{-2}$ (Fig. 1b). Because lateral channel migration rates are low in

the downstream reaches of the Bermejo (Repasch, 2023; Repasch et al., 2020) it is unlikely that local C4 plants

will make it into the bedload in any significant quantities. Finding signatures of C4 plants in downstream lowland

410 bedload samples provide evidence for long-range transport of POM$_{Bed}$ from the Bermejo headwaters to nearly

1000 km downstream.

$n$C$_{29}$ $\delta^2H$ values can serve as a proxy for the local meteoric water composition taken up by plants, as it

is influenced by the water incorporated into plants during photosynthesis (Sachse et al., 2012; Hou et al., 2008;

415 Chikaraishi et al., 2004), and are strongly related to temperature, humidity, rainfall amount, moisture source, and

elevation (e.g.,Walker and Richardson, 1991; Allison et al., 1984; Stewart and Taylor, 1981). In our study area,

increasing altitude causes decreasing $\delta^2H$ values in meteoric water captured in plant tissue: More negative $\delta^2H$

values corresponded to higher elevations. Nieto-Moreno et al. (2016) measured soil $n$C$_{29}$ $\delta^2H$ values ranging from

-150 to -110‰ in samples collected along a valley transect ranging from ~300 to ~4000 m in elevation at a

420     headwater tributary of the Rio Bermejo between 22 and 24°S, and the same pattern was described for stream water $\delta^2H$ values in this region (Rohrmann et al., 2014). Our samples follow these systematics, with $\delta^2H$ values averaging -136±15‰ (range: -155 - -112‰, n = 13), for leaf litter sampled at ~270 – 320 m elevation in the Chaco lowland, and more negative $\delta^2H$ values in both leaf litter (-168±21‰, range: -187 - -130‰, n = 9) and $POM_{float}$ (-160±7‰, range: -171 - -153‰, n = 5) collected upstream of the confluence.

425     $^2H$ depletion correlates significantly with increasing elevation in floodplain and headwater leaf litter samples (Fig. 6, y = -640 – 6.4x, $R^2$ = 0.557, p < 0.01). This is true also for the $POM_{float}$ samples, however, not significantly (y = -3606-30x, $R^2$ = 0.14 , p > 0.05). The sampling transect for $POM_{float}$ covers a rapid westward precipitation decline, where samples from >1000 m asl. are likely sourced from arid areas, whereas the samples from lower elevations receive orographic precipitation, suggesting that the gradient in precipitation amount may cause the

430     observed $^2H$ depletion and the worse fit in $POM_{float}$ samples.

Nevertheless, the elevation dependent $\delta^2H$ composition is caused by a precipitation-dependent change in $\delta^2H$ values of the areas covered by our study, as shown by Nieto-Moreno et al. (2016) and Rohrmann et al. (2014): upland areas are depleted in $^2H$ compared to the Rio Bermejo lowland, where convective precipitation is the main source of moisture (Rohrmann et al., 2014). We take advantage of this elevation-dependent trend in source POM

435     $\delta^2H$ values to identify source elevations of the $POM_{Bed}$ samples, where more negative $\delta^2H$ values indicate a higher elevation origin, and less negative $\delta^2H$ values signal a low elevation floodplain origin. $POM_{Bed}$ samples do not show such a correlation of sampling elevation with $\delta^2H$ values, and we suggest this is due to transport between production and sampling of this material.

### 4.2.2 Mixing model analysis

440     We defined three potential $POM_{Bed}$ sources, from coarse organic debris we sampled at distinct elevations in the catchment: floodplain leaf litter (<320 m), headwater leaf litter (320-1000 m) and headwater $POM_{float}$ (>320 m). Significant end-member unmixing of the respective sources to the mixed $POM_{Bed}$ signal is not expedient using the geochemical proxies applied in this study. Instead, we aim to understand the mixing range of the widely spread

445     $POM_{Bed}$. We determine the range of a possible $POM_{Bed}$ mixing signal of the sources within the geochemical parameters, and in addition, determine potential missing $POM_{Bed}$ sources. We use a mixing-space model developed by (Smith et al., 2013a). In short, the model uses Monte Carlo simulations to iterate mixing spaces (="convex hulls") outlining the probability that observed $POM_{Bed}$ sample compositions can be explained by a mixing model of the proposed sources. The model utilizes resampled source averages and their standard

450     deviations, and considers the distribution of the mix data (=$POM_{Bed}$ data) within a pre-defined mixing space.

For our purpose, we assume uniform source mixing of the $POM_{Bed}$ samples, without fractionation from the source composition of $POM_{float}$, floodplain, and headwater leaf litter $\delta^2H$ /$ACL_{25-33}$ and $\delta^2H$ /$\delta^{13}C$ to $POM_{Bed}$. We use minimum and maximum boundary conditions based on our source data to define the extent of the initial mixing space: 25 to 35 for the $ACL_{25-33}$, -190 and -110‰ for $\delta^2H$ values, and -40 and -20‰ for $\delta^{13}C$ values. The initial

455     mixing space is iteratively adapted over 2000 iterations, using source data average and standard deviation, resampled from a normal distribution. Through each iteration, a point-in-polygon algorithm tests if the mixed $POM_{Bed}$ data remains within the iteratively adapted mixing space. This ensures an "optimization" of the mixing space according to our $POM_{Bed}$ data, permitting to evaluate if the actual $POM_{Bed}$ sources are not fully represented by our included sources. The point-in-polygon algorithm is applied to a testing grid within the mixing space. With

460  a grid resolution of 500 ‰$^2$, the point-in-polygon is tested on 500×500 values per iteration within the mixing region. Simultaneously, the area of the mixing space is assessed, and the variance between all previous iterations calculated. The stabilized variance value, then, represents the optimized mixing space area for the available source data and the mixed POM$_{Bed}$ data.

The variance of the convex hull area stabilized after ~1000 iterations for the $\delta^2$H /ACL$_{25-33}$ model, at a variance

465  of 40 ‰$^2$, and after ~1000 iterations for $\delta^2$H /$\delta^{13}$C at a variance of 60 ‰$^2$. The resulting mixing regions were not sensitive to variations of the boundary conditions. The results are plotted as derived mixing regions, with different levels of confidence representing the likelihood with which the observed data can result from mixing of the source
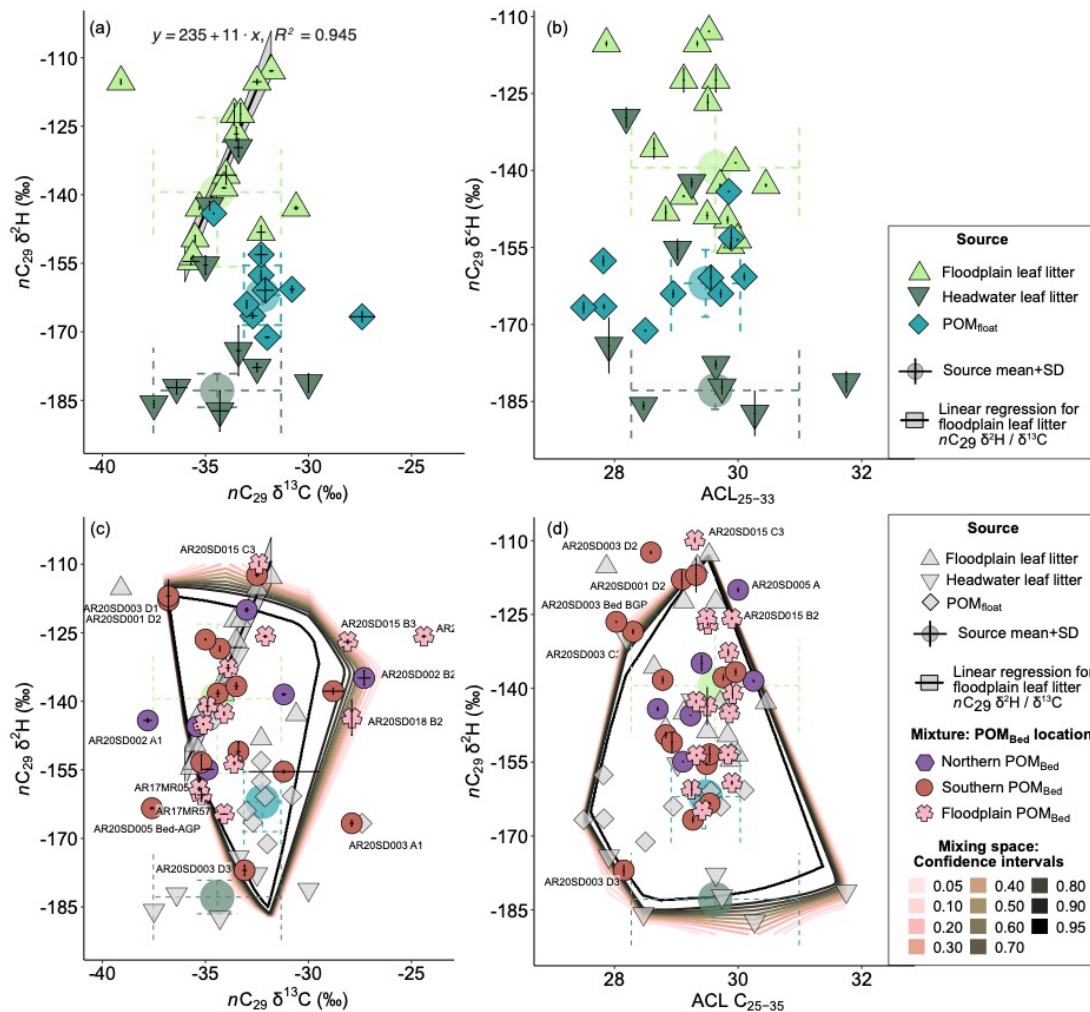
**Figure 7:** Upper panels: Headwater and floodplain leaf litter and POM$_{float}$ samples, average ± standard deviation, depicted as potential POM$_{Bed}$ sources, using (a) $n$C$_{29}$ $\delta^2$H versus $n$C$_{29}$ $\delta^{13}$C and (b) $n$C$_{29}$ $\delta^2$H versus ACL$_{25-33}$. Lower panels: Greyed out area symbols and colored averages correspond to the OM sources from panels a and b. Colored symbols are POM$_{Bed}$ samples from headwaters and floodplain, for (a) $n$C$_{29}$ $\delta^2$H versus $n$C$_{29}$ $\delta^{13}$C, and (b) $n$C$_{29}$ $\delta^2$H versus ACL$_{25-33}$. Colored lines are probability contours of the simulated mixing area (Smith et al., 2013a), using the organic matter source. Outermost contour represents the 5%, innermost contour the 95% confidence level. Labelled POM$_{Bed}$ samples are those that fall outside the mixing area and the source area of both plots. Uncertainty is plotted inside the symbol. Linear regression in plot a and c was conducted using lowland leaf litter data.

data (Fig. 7).

**4.2.3 Mixing model insights into POM_Bed source areas**

We proceed to use floodplain leaf litter, headwater leaf litter, and headwater POM_float ACL$_{25-33}$/$n$C$_{29}$ $\delta^2$H, $n$C$_{29}$ $\delta^{13}$C/$n$C$_{29}$ $\delta^2$H values as potential sources to create mixing regions for our POM_Bed samples (Fig. 7a, b). Half of the samples follow the $\delta^2$H/$\delta^{13}$C compositional trend of leaf litter (y =-234.8x+10.8, R$^2$ = 0.94), with $n$C$_{29}$ $\delta^2$H values ranging from -174 - -112‰, and $\delta^{13}$C values ranging from -39.0‰ - -30.0‰ (Fig. 7c). This indicates that locally supplied floodplain leaf litter is an important source to the sampled POM_Bed, as already suggested earlier. In these samples, this lowland-derived plant material dominates over any existing bedload sourced from upstream areas.

Twenty percent of the POM_Bed samples fall within the region of the $n$C$_{29}$ $\delta^{13}$C/$n$C$_{29}$ $\delta^2$H mixing space defined by headwater sources. This suggests input from at least one high elevation upland source. Evidence for this high elevation OM source in lowland POM_Bed samples confirms that mountain-derived OM can survive long-range bedload transport in the Rio Bermejo.

One third of the POM_Bed samples fall outside the 95% confidence interval of the $\delta^2$H/$\delta^{13}$C mixing space, while some POM_Bed samples collected from both the headwaters and the lowland are not within the wider mixing space constrained by $\delta^2$H /ACL$_{25-33}$ (Fig. 7c, d). These samples have $n$C$_{29}$ $\delta^2$H values ranging from -125 - -150‰ and $n$C$_{29}$ $\delta^{13}$C values ranging from -27 - -33‰ (see labelled POM_Bed samples in Fig. 7). This suggests input from at least one additional, herein unconstrained source, and the comparably heavy $\delta^{13}$C values suggest this could contain C4 plant contributions. C4 plants grow only sparsely in the catchment (Fig. 1b), and mostly on agricultural land in HW_South. We suggest that the missing source in our samples is farmland OM, which would indicate that the POM_Bed carbon flux can be directly influenced by anthropogenic land use.

Sediment load data from gauging stations on the upper Rio Bermejo and Rio San Francisco indicate that HW_North contributes six times more suspended sediment load to the lowland Rio Bermejo than HW_South (Repasch et al., 2020). There is a north to south rainfall gradient with almost three times more precipitation in HW_North (Fig. 1c, Hijmans et al., 2005), indicating higher erosion potential and possibly causing more recruitment of organic bedload from this area (Galy et al., 2015). This suggests that the HW_North source area should dominate organic input from the headwaters. However, this cannot be constrained with the geochemical proxies adopted in this study.

**4.3 Long-range transport of POM_Bed**

Recent studies show that fresh, coarse organic debris can generally be found near the river bed (Repasch et al., 2022; Schwab et al., 2022; Feng et al., 2016), but the implications of this transport for the OC cycle are underconstrained. Using our new understanding of the POM_Bed source areas and the evolution downstream, we now consider the fate of POM_Bed during long-range fluvial transport through the Rio Bermejo lowland river system.

The proportion of POM transported at the bed versus in suspension is a function of particle size, density and shape, the recalcitrance of the POM, the river's turbulence, sediment load, the flow close to the bed (Turowski et al., 2016; Nichols et al., 2000), and secondary flow motions (Schwab et al., 2022). Assuming that POM_Bed moves as clastic bedload, with a pace of about 0.7 times the depth-averaged flow velocity (Chatanantavet et al., 2013), which is around 0.46 m s$^{-1}$ (average of positive flow velocities, Table S01) at both the Bermejo-San Francisco confluence and downstream locations alike. At this velocity, a POM_Bed parcel could be transported 1300

510    km through the Rio Bermejo floodplain in ~45 days. Moreover, slightly higher $CPI_{25-33}$ values at downstream sites (average: 8.2±3.0, range 4.9-15.2, n = 14, Fig. 5) versus upstream (average: 6.9±3.0, range 0.1-11.7, n = 25, Fig. 5) suggest there is no systematic, progressive degradation of $POM_{Bed}$ during long-range fluvial transport, likely because transport timescales are too short to produce significant chemical degradation. This demonstrates that $POM_{Bed}$ can travel from the Andean headwaters into the Rio Paraguay within one single high flow season in the

515    Rio Bermejo. It explains the absence of $POM_{Bed}$ during the low flow season when little OM is likely to come in from outside the river channel. Moreover, it elucidates the occurrence of coarse organic debris in turbidity currents and turbidite deposits, where it is buried under finer clastic sediments (Hage et al., 2020; Lee et al., 2019; McArthur et al., 2016; Sparkes et al., 2015).

520    Once entrained, $POM_{Bed}$ likely moves as semi-separate layer in deep and fast flowing parts of the channel cross section where bed shear stress is greatest. Without substantial mixing, parcels of $POM_{Bed}$ may shuffle downstream due to discrete erosion events at high flow and deposition at low flow. Episodic flushing events of the channel can transport parcels efficiently (Heijnen et al., 2022), and facilitate waterlogging of the organic debris (West et al., 2011). Waterlogged coarse organic debris is not prone to spilling onto the river bank or across levees

525    into adjacent flood basins and can progress downstream. Thus, the downstream advection of $POM_{Bed}$ in the Rio Bermejo may be sustained by seasonal high flow driven by monsoonal rainfall and quasi-uninterrupted by intermittent deposition. The helical flow induced by the constant meandering of the lower Rio Bermejo could augment this process (Schwab et al., 2022). As such, significant amounts of OM could be efficiently transported with bedload through large drainage basins, from mountainous uplands to marine basins on sub-seasonal

530    timescales.

### 4.3.1 Mechanical comminution of $POM_{Bed}$ during long-range transport

Despite evidence for survival during long-range fluvial transport, we might expect that the physical interaction between bedload OM and clastic particles can cause comminution of organic particles (Dosch et al.,

535    2021; Scheingross et al., 2019; Turowski et al., 2016; Hilton et al., 2012; Attal and Lavé, 2009; Nichols et al., 2000), and that comminuted $POM_{Bed}$ transfers into the river suspended load. The observed decrease in $POM_{Bed}$ sample size with increasing distance downstream from the confluence suggests a progressive loss of $POM_{Bed}$ (Fig. 4d), despite the input of OM from lateral erosion of the lowland floodplain. The similarity between $n$-alkane $\delta^{13}C$, $\delta^{2}H$, and $ACL_{25-33}$ values of the Rio Bermejo suspended sediment and $POM_{Bed}$ (Fig. 5) implies that the two

540    fractions share an origin. River suspended sediment samples yielded similar $CPI_{25-33}$ values, on average 5.5±1.0 (range: 1.1-7.8; n = 41), but with less variability and values only as high as 7.8, suggesting advanced mixing and maturity compared to $POM_{Bed}$ (average: 29.6±0.9, range 27.4-31.6, n =39).

The particle size distributions of $POM_{Bed}$ samples from downstream locations were considerably finer

545    than samples from the confluence, even if the recovered sample sizes did not permit separation of aliquots for grainsize measurements. As flow velocities increase, $POM_{Bed}$ particles may increasingly transfer into suspension, rather than traveling at the river bed (Turowski et al., 2016). This transition is smooth, and $POM_{Bed}$ may move in saltation at the transition between the two transport modes (e.g., Turowski et al., 2016; Nichols et al., 2000). However, flow velocities along the Rio Bermejo mainstem show no significant variability, therefore, transfer from

POM_Bed to the suspended load is more likely to result from the comminution of coarse particles, rather than changes in river hydrodynamics. To our knowledge, there are no experimental or field data showing comminution of particulate organic matter. However, Merten et al. (2013) suggested that physical breakage of large woody debris in streams is likely dominantly controlled by the structural properties and position in-stream of the organic matter, as opposed to hydraulic and geomorphic variables, concurring with our interpretation. Further research is needed to determine the scope and controlling factors of physical decay of coarse organic matter in the water column.

**5 Synthesis: Bedload carbon fluxes at the Rio Bermejo**

We close with a provisional examination of the organic carbon flux associated with bedload transport, its relation to suspended transport, and its role in the terrestrial carbon cycle. We extrapolated our local, high flow season point measurements of POM_Bed across the respective river transects, ignoring any OM particles <1 mm in near-bed transport, and used a simple upscaling approach to estimate the flux of organic carbon with bedload POC_Bed (in tC yr$^{-1}$).

$$POC_{Bed} = \frac{\sum POM_{Bed} \times 0.58}{t_{sampling}} \times \frac{\text{Transect width} \times 0.5}{\text{Funnel width}} \times t_{transport}$$ (3).

We sum the sampled POM_Bed (POM_Bed >1 mm, in mass × min$^{-1}$), apply the van Bemmelen factor, 0.58, to represent the carbon content in (soil) organic matter (Allison, 1965), and divide by the sampling time $t_{sampling}$ (in min) along each transect, using the respective standard deviation of POM_Bed to define an upper and lower boundary of the estimated bedload carbon flux. To do this, we extrapolated the samples obtained with a funnel opening of 0.08 m to the central 50% of the river channel (transect width × 0.5, in m$^2$), where assumed that POM_Bed transport is concentrated. Since we did not capture significant amounts of POM_Bed during the dry season, we assumed that POM_Bed transport only occurs during the six months of the high flow season ($t_{transport}$ = 182.5 days). This approach allowed us to estimate POC_Bed without using near-bed velocities that were not available for all locations.

HW_North and HW_South both show an increase in the POM_Bed flux from the upper headwater locations (HW_North-2 and HW_South-2, respectively) to the lower headwater locations (HW_North-1 and HW_South-1, respectively), demonstrating the possibility of fast recruitment of POM_Bed on short distances. To determine changes in mass flux from the mountain front to the downstream reaches, we compare the combined headwater fluxes to those estimated at downstream sampling sites. The fluxes of POM_Bed at the upper Rio Bermejo at HW_North-1 and Rio San Francisco at HW_South-1 define the flux into the low-gradient portion of the river. We estimate the POM_Bed fluxes from HW_South and HW_North at 926-1138 tC yr$^{-1}$ and 112-188 tC yr$^{-1}$, respectively, for a total of 1038-1326 tC yr$^{-1}$ exported from the headwaters to the lowland reach (Fig. 8, Table 2). Downstream at LL-1, we calculate a POM_Bed flux of 155-351 tC yr$^{-1}$, while at LL-2 we estimate 19-27 tC yr$^{-1}$.

**Table 2:** Bedload sampling locations and yields from the field campaign in 2020, and estimated flux of particulate organic carbon on the river bed.

| Location name | Sampling time $t_{sampling}$ | Total sum bedload | Total sum $POM_{Bed}$ >1 mm | Full transect width | Average near-bed flow velocity ± standard deviation [a] | $POC_{Bed}$ flux ± standard deviation [c] |
|---|---|---|---|---|---|---|
| | (min) | (g) | (g) | (m) | (m s$^{-2}$) | (tC yr$^{-1}$) |
| HW$_{South-2}$ (Caimancito) | 2 | 588 | 22 | 80 | NA | 855 ± 513 |
| HW$_{North-1}$ (Embarcacion) | 4 | 2589 | 5 | 169 | 0.29 ± 0.3 | 150 ± 38 |
| HW$_{South-1}$ (Pichanal) | 11 | 7283 | 66 | 183 | 0.49 ± 0.3 | 1032 ± 106 |
| HW$_{North-2}$ (Rio Colorado) | 4 | 955 | 3 | 35 | NA | 11 ± 1 |
| LL$_{-1}$ (Puerto Lavalle) | 7 | 617 | 9 | 215 | -0.19 ± 0.4 | 253 ± 98 |
| LL$_{-2}$ (El Colorado) | 5 | 617 | 1 | 90 | 0.27 ± 0.6 | 23 ± 4 |

[a] Measured using ADCP. [b] Averaged per number of samples per sampling site. [c] Calculated using Equation 3.

It is difficult to reconcile the minimum 66% loss of C in bedload between the Bermejo-San Francisco confluence and LL$_{-1}$ (865 km transport distance) with the subsequent large apparent 10-fold reduction of the bedload C flux from LL$_{-1}$ to LL$_{-2}$, over a transport distance of only ~220 km. The downstream increase of POM$_{Bed}$ aggregates that dissociated into POM$_{Bed}$ <1 mm, could cause an underestimation of the POM$_{Bed}$ >1 mm flux at LL$_{-2}$. The discrepancy may further be due to sampling bias (Turowski et al., 2013), bedload flux variability due to bedforms, the formation of OM waves at the channel bed, interspersed with relatively barren intervals (Heijnen et al., 2022), strongly sustained by discharge (e.g., Rickenmann, 2018; Turowski et al., 2016; Reid et al., 1998), and channel geometry (Fogel and Lininger, 2023). Bedload sampling, particularly using Helley-Smith samplers, can be prone to high variability, and we suggest our estimates are an order-of-magnitude approximation (Bunte et al., 2008) that likely underestimates the maximum POM$_{Bed}$ transport rate. This could also cause the flux rates of HW$_{South}$ that exceed the fluxes at HW$_{North}$, despite the higher erosive potential at HW$_{North}$. Higher agricultural activities in HW$_{South}$ could also enhance surface erosion, and with that OM input locally. Our approach assumes that the dimension of the POM$_{Bed}$ layer, and its individual particles are within the constraints of the funnel height of the sampler, and that the samples and sampling points across each transect represent the cross-section of the channel. A larger samples size, and sampled surfaces area, longer sampling times, and better understanding of distribution and dynamics of the POM$_{Bed}$ layer could greatly enhance the accuracy of the sample set and flux estimates. Despite these uncertainties, this is the first estimate of its kind, and shows that river POM fluxes may be underestimated without considering the bedload OM flux.

The inferred POM$_{Bed}$ grain size reduction during transport, similar to clastic sediment (Attal and Lavé, 2009), contributes to the overall suspended sediment yield of the river. The total suspended organic carbon flux is ~$1.85×10^5$ tC yr$^{-1}$ at the Bermejo-San Francisco confluence (Repasch et al., 2021), suggesting that the estimated POM$_{Bed}$ carbon flux near the confluence is less than 1% of the total carbon load. The Rio Bermejo exports ~$2.24×10^5$ tC yr$^{-1}$ in suspension downstream to the Rio Paraguay, implying that about $0.39×10^5$ tC yr$^{-1}$ of suspended organic carbon are delivered to the lowland channel by lateral erosion (Repasch et al., 2021). If we take the downstream estimates of bedload C flux at face value, and assume this loss transfers to the suspended load, a mass balance suggests that less than 1% of the suspended load gain between the confluence and LL$_{-1}$ and LL$_{-2}$ could be due to grain size reduction of the coarse organic load. While our bedload carbon flux estimates are

620 tentative, it is clear that this eye-catching mode of organic carbon transfer is small in comparison with the fluvial export of organic carbon in the suspended load of the Rio Bermejo.

However, the Rio Bermejo's suspended sediment yield is exceptionally high (Sambrook Smith et al., 2016). Assuming the loss between the $HW_{South-1}$+ $HW_{North-1}$ and $LL_{-1}$ and $LL_{-2}$ transfers completely to the suspended load, 79% and 98%, respectively of $POM_{Bed}$ would transfer into suspension, while simultaneously

625 recruiting additional bedload from the floodplain. $POM_{Bed}$ in rivers and sedimentary deposits could contribute substantially to the overall flux in river systems with lower suspended sediment yield, and where bedload dominates the fluvial sediment flux (Turowski et al., 2016), or in highly erosive headwater streams with short transport distances from recruitment to subsequent deposition and burial (Blair and Aller, 2012; Hilton et al., 2011).

630

This coarse particulate OM may also have a higher probability of preservation and rapid burial in depositional basins, as its particle settling velocity is higher than smaller particles and may be less prone to resuspension and oxidation. Future work should aim to enhance our understanding of the significance of $POM_{Bed}$ export and burial over varying transport length scales.

635
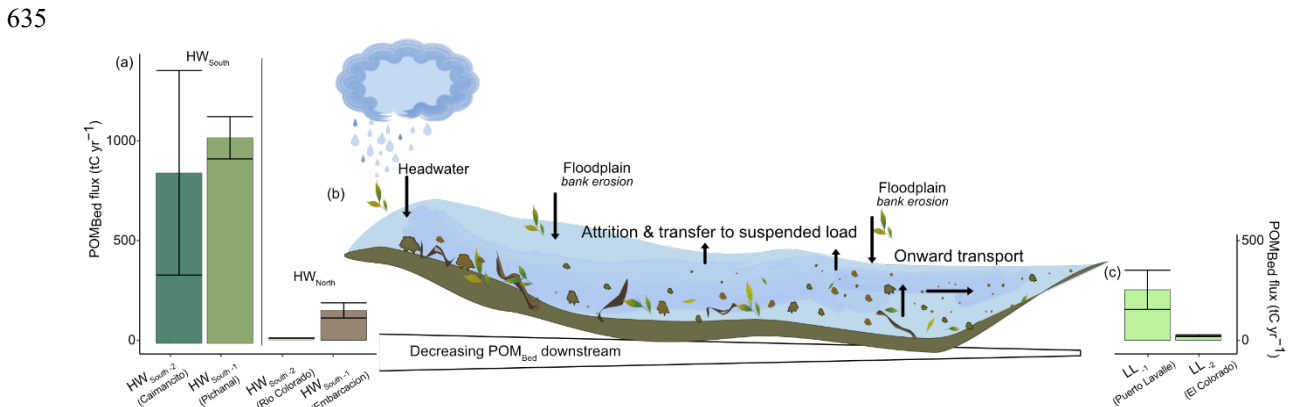
**Figure 8:** (a) Barplot showing the order of magnitude estimates (± standard deviation) of the $POM_{Bed}$ flux (tC yr$^{-1}$) at $HW_{South}$ and $HW_{North}$. (b) Illustration of the source areas, transport and fate of $POM_{Bed}$ at the Rio Bermejo from upstream recruitment downstream: Sourcing from the headwater and the floodplain during wet season erosion, partial attrition and transfer to suspended load, causing a net decrease in $POM_{Bed}$, and onward transport of the remaining $POM_{Bed}$, leading to (c) order of magnitude estimates of the lowland $POM_{Bed}$ flux (tC yr$^{-1}$).

**6 Conclusion**

In this study, we investigated the occurrence, recruitment mechanisms, source areas, and survival of $POM_{Bed}$ during long-range transport, to understand the implications for the terrestrial organic carbon cycle. We found the persistent occurrence of $POM_{Bed}$ along a 1300 km section of the Rio Bermejo in northern Argentina,

640 from the headwaters to its confluence with the Rio Paraguay.

Our results provide evidence that the $POM_{Bed}$ originates from erosion of fresh, terrestrial organic debris from the local floodplain, as well as distal headwater sources, and is composed of a heterogenous mix from catchment-wide sources, dominated by C3 plant input, and local C4 point sources. $POM_{Bed}$ can remain geochemically unaltered over long fluvial transport distances, due to fast transport. The high geochemical variability within and

645 between the bedload sampling transects (Fig. S2) does not allow a quantitative unmixing of $POM_{Bed}$ sources; however, this variability indicates that $POM_{Bed}$ may travel in parcels, each representing an erosive event that delivered fresh OM to the river, where it was subsequently waterlogged and translocated to the channel bed. Our

data suggest coherent and continuous transport of individual OM parcels at the river bed, such that $POM_{Bed}$ is never fully mixed longitudinally in a river system. Although $POM_{Bed}$ appears to survive long-range fluvial transport, it can mechanically break down during transport, contributing to the overall suspended sediment load of the river. After physical breakdown, the fate of $POM_{Bed}$ does not lay exclusively in the suspended fraction. The geochemical proxies of the Rio Bermejo soil and bank sediment suggest it can also be stored on floodplains and undergo partial mineralization. Changes in hydraulic settings can lead to particle settling, and high suspended sediment yields enhance the burial efficiency and promote drawdown of atmospheric $CO_2$ over longer timescales.

The decreasing $POM_{Bed}$ flux downstream also indicates that the loss of $POM_{Bed}$ exceeds the recruitment from the floodplain and therefore, that local ecosystem productivity is likely not the main factor controlling $POM_{Bed}$ genesis at the Rio Bermejo. Rather, the main control is likely to be the preconditioning of OM, such that it can rapidly absorb water, increasing its density and its settling velocity, allowing it to sink (Hoover et al., 2010). Overland flow is also necessary to facilitate OM erosion and transport to the active channel, and sufficient river flow velocity is required to maintain transport at the bed (Galy et al., 2015). Likewise, the ratio of $POM_{Bed}$ export and potential burial versus abrasion and transport as suspended sediment likely dependents on plant type, climate, river morphology, hydrodynamics, and transit time (Hoover et al., 2010).

We found that transport of $POM_{Bed}$ is not a major contributor to carbon burial on short timescales at the Rio Bermejo, but ongoing floodplain recruitment contributes to the genesis of $POM_{Bed}$, and fluvial transport could export $POM_{Bed}$ from the headwaters to the ocean on short timescales, representing a hitherto under-investigated mechanism for fluvial organic carbon export and burial. Bedload transport can convey OM to downstream basins with subsequent burial over millennial timescales, however, possibly more significant on shorter transport-distances. The abundance and magnitude of bedload is in general highly variable and notoriously difficult to measure, and it remains challenging to quantify the total amount of $POM_{Bed}$, due to stochasticity of bedload transport and the heterogeneity of $POM_{Bed}$ abundance. Our approach is a first step to evaluate the origin and fate of $POM_{Bed}$ during long-range fluvial transport in a natural setting. Further experimental and field studies are necessary to improve our understanding of the fraction of POM transported as bed material versus in the water column.

**Data availability**

Additional data referred to in the main text, data tables and mode code are available in the supporting information file: https://doi.org/10.5880/GFZ.4.6.2023.005.

**Author Contributions**

**Conceptualization:** Sophia Dosch, Niels Hovius, Marisa Repasch, Joel S. Scheingross, Jens Turowski, Dirk Sachse

**Formal analysis:** Sophia Dosch

**Funding acquisition:** Niels Hovius, Dirk Sachse

**Investigation:** Sophia Dosch, Niels Hovius, Marisa Repasch, Stefanie Tofelde, Dirk Sachse

**Methodology:** Marisa Repasch, Niels Hovius, Oliver Rach, Jens Turowski, Dirk Sachse

**Conflicts of Interest**

At least one of the (co-)authors is a member of the editorial board of Earth Surface Dynamics

**Acknowledgments**

This research was funded by the Deutsche Forschungsgemeinschaft (DFG) and the Federal State of Brandenburg under the auspices of the International Research Training Group IGK2018 "SuRfAce processes, TEctonics and Georesources: The Andean foreland basin of Argentina" (STRATEGy), DFG grant STR 373/34-1 to M. Strecker. Figures were produced with R ggplot2, Version 3.4.0.

References

Allen, J. R. L.: Current Ripples. Their relation to patterns of water and sediment motion, Geological Magazine, 106, 614-614, 10.1017/S001675680005946X, 1968.

700

Allen, G. P., Laurier, D., and Thouvenin, J.: Étude sédimentologique du delta de la Mahakam, Compagnie Française des Pétroles. Notes et Mémoires, 156, 1979.

Aller, R. C.: Mobile deltaic and continental shelf muds as suboxic, fluidized bed reactors, Marine Chemistry, 61, 143-155, https://doi.org/10.1016/S0304-4203(98)00024-3, 1998.

705

Allison, G. B., Barnes, C. J., Hughes, M. W., and Leaney, F. W. J.: Effect of climate and vegetation on oxygen-18 and deuterium profiles in soils, IAEA, International Atomic Energy Agency (IAEA)1984.

710   Allison, L. E.: Organic Carbon, in: Methods of Soil Analysis, 1367-1378, https://doi.org/10.2134/agronmonogr9.2.c39, 1965.

Attal, M. and Lavé, J.: Pebble abrasion during fluvial transport: Experimental results and implications for the evolution of the sediment load along rivers, Journal of Geophysical Research, 114, 10.1029/2009jf001328, 715   2009.

Battin, T. J., Luyssaert, S., Kaplan, L. A., Aufdenkampe, A. K., Richter, A., and Tranvik, L. J.: The boundless carbon cycle, Nature Geoscience, 2, 598-600, 10.1038/ngeo618, 2009.

720   Berner, R. A.: Burial of organic carbon and pyrite sulfur in the modern ocean- Its geochemical and environmental significance, American Journal of Science, 282, 451-473, 10.2475/ajs.282.4.451, 1982.
Blair, N. E. and Aller, R. C.: The fate of terrestrial organic carbon in the marine environment, Ann Rev Mar Sci, 4, 401-423, 10.1146/annurev-marine-120709-142717, 2012.

725   Blattmann, T. M., Liu, Z., Zhang, Y., Zhao, Y., Haghipour, N., Montlucon, D. B., Plötze, M., and Eglinton, T. I.: Mineralogical control on the fate of continentally derived organic matter in the ocean, Science, 366, 742-745, 10.1126/science.aax5345, 2019.

Bouchez, J., Galy, V., Hilton, R. G., Gaillardet, J., Moreira-Turcq, P., Pérez, M. A., France-Lanord, C., and 730   Maurice, L.: Source, transport and fluxes of Amazon River particulate organic carbon: Insights from river sediment depth-profiles, Geochimica et Cosmochimica Acta, 133, 280-298, 10.1016/j.gca.2014.02.032, 2014.

Bray, E. E. and Evans, E. D.: Distribution of n-pamlEns as a clue to recognition of source beds, Geochimica et Cosmochimica Acta, 22, 2-15, https://doi.org/10.1016/0016-7037(61)90069-2, 1961.

735

Bunte, K., Abt, S. R., Potyondy, J. P., and Swingle, K. W.: A Comparison of Coarse Bedload Transport Measured with Bedload Traps and Helley-Smith Samplers, Geodinamica Acta, 21, 53-66, 10.3166/ga.21.53-66, 2008.

740   Bunte, K., Swingle, K. W., Turowski, J. M., Abt, S. R., and Cenderelli, D. A. A.: Measurements of coarse particulate organic matter transport in steep mountain streams and estimates of decadal CPOM exports, Journal of Hydrology, 539, 162-176, 10.1016/j.jhydrol.2016.05.022, 2016.

Canuel, E. A. and Hardison, A. K.: Sources, Ages, and Alteration of Organic Matter in Estuaries, Annual Review 745   of Marine Science, 8, 409-434, 10.1146/annurev-marine-122414-034058, 2016.

Chatanantavet, P., Whipple, K. X., Adams, M. A., and Lamb, M. P.: Experimental study on coarse grain saltation dynamics in bedrock channels, Journal of Geophysical Research: Earth Surface, 118, 1161-1176, 10.1002/jgrf.20053, 2013.

750

Chikaraishi, Y., Naraoka, H., and Poulson, S. R.: Hydrogen and carbon isotopic fractionations of lipid biosynthesis among terrestrial (C3, C4 and CAM) and aquatic plants, Phytochemistry, 65, 1369-1381, 10.1016/j.phytochem.2004.03.036, 2004.

755 Collister, J. W., Rieley, G., Stern, B., Eglinton, G., and Fry, B.: Compound-specific δ 13C analyses of leaf lipids from plants with differing carbon dioxide metabolisms, Organic Geochemistry, 21, 619-627, https://doi.org/10.1016/0146-6380(94)90008-6, 1994.

Cranwell, P. A.: Chain-length distribution of «-alkanes from lake sedimentsin relation to post-glacial
760 environmental change, Freshwater Biology, 2, 259–265, 1972.

Dellinger, M., Hilton, R. G., Baronas, J. J., Torres, M. A., Burt, E. I., Clark, K. E., Galy, V., Ccahuana Quispe, A. J., and West, A. J.: High Rates of Rock Organic Carbon Oxidation Sustained as Andean Sediment Transits the Amazon Foreland-Floodplain, Proceedings of the National Academy of Sciences, 10.1073/pnas.2306343120,
765 2023.

Dosch, S., Hovius, N., Repasch, M., Scheingross, J., Turowski, J., and Sachse, D.: Terrestrial biospheric carbon export from rivers by bedload transport, EGU General Assembly 2021, online, 19–30 Apr 2021, https://doi.org/10.5194/egusphere-egu21-10684, 2021.
770
Feng, X., Feakins, S. J., Liu, Z., Ponton, C., Wang, R. Z., Karkabi, E., Galy, V., Berelson, W. M., Nottingham, A. T., Meir, P., and West, A. J.: Source to sink: Evolution of lignin composition in the Madre de Dios River system with connection to the Amazon basin and offshore, Journal of Geophysical Research: Biogeosciences, 121, 1316-1338, 10.1002/2016jg003323, 2016.
775
Fogel, C. B. and Lininger, K. B.: Geomorphic complexity influences coarse particulate organic matter transport and storage in headwater streams, Frontiers in Water, 5, 10.3389/frwa.2023.1227167, 2023.

France-Lanord, C. and Derry, L. A.: Organic carbon burial forcing of the carbon cycle from Himalayan erosion,
780 Nature, 390, 65-67, 10.1038/36324, 1997.

Freeman, K. H. and Colarusso, L. A.: Molecular and isotopic records of C4 grassland expansion in the late Miocene, Geochimica et Cosmochimica Acta, 65, 1439–1454, 10.1016/s0016-7037(00)00573-1, 2001.

785 Galy, V., France-Lanord, C., and Lartiges, B.: Loading and fate of particulate organic carbon from the Himalaya to the Ganga–Brahmaputra delta, Geochimica et Cosmochimica Acta, 72, 1767-1787, 10.1016/j.gca.2008.01.027, 2008.

Galy, V., Peucker-Ehrenbrink, B., and Eglinton, T.: Global carbon export from the terrestrial biosphere
790 controlled by erosion, Nature, 521, 204-207, 10.1038/nature14400, 2015.

Galy, V., Eglinton, T., France-Lanord, C., and Sylva, S.: The provenance of vegetation and environmental signatures encoded in vascular plant biomarkers carried by the Ganges–Brahmaputra rivers, Earth and Planetary Science Letters, 304, 1-12, 10.1016/j.epsl.2011.02.003, 2011.
795
Garcia, C., Laronne; J. B., and Sala, M.: Variable source areas of bedload in a gravel-bed stream, J Sediment Res, 69, 27-31, 1999.

Garcin, Y., Schefuß, E., Schwab, V. F., Garreta, V., Gleixner, G., Vincens, A., Todou, G., Séné, O., Onana, J.-M.,
800 Achoundong, G., and Sachse, D.: Reconstructing C 3 and C 4 vegetation cover using n -alkane carbon isotope ratios in recent lake sediments from Cameroon, Western Central Africa, Geochimica et Cosmochimica Acta, 142, 482-500, 10.1016/j.gca.2014.07.004, 2014.

Golombek, N., Scheingross, J. S., Repasch, M. N., Hovius, N., Sachse, D., Lupker, M., Eglinton, T. I., Menges,
805 J., Haghipour, N., Poulson, S. R., Gröcke, D. R., Latosinski, F. G., and Szupiany, R. N.: Seasonal variability of fluvial organic carbon composition between 2016-2018 in the Río Bermejo, Argentina, 10.1594/PANGAEA.932558, 2021.

Hage, S., Galy, V. V., Cartigny, M. J. B., Acikalin, S., Clare, M. A., Gröcke, D. R., Hilton, R. G., Hunt, J. E.,
810 Lintern, D. G., McGhee, C. A., Parsons, D. R., Stacey, C. D., Sumner, E. J., and Talling, P. J.: Efficient preservation of young terrestrial organic carbon in sandy turbidity-current deposits, Geology, 48, 882-887, 10.1130/g47320.1, 2020.

Hage, S., Galy, V. V., Cartigny, M. J. B., Heerema, C., Heijnen, M. S., Acikalin, S., Clare, M. A., Giesbrecht, I., Gröcke, D. R., Hendry, A., Hilton, R. G., Hubbard, S. M., Hunt, J. E., Lintern, D. G., McGhee, C., Parsons, D. R., Pope, E. L., Stacey, C. D., Sumner, E. J., Tank, S., and Talling, P. J.: Turbidity currents can dictate organic carbon fluxes across river-fed fjords: An example from Bute Inlet (BC, Canada), Journal of Geophysical Research: Biogeosciences, 10.1029/2022jg006824, 2022.

Hayes, J. M., Strauss, H., and Kaufman, A. J.: The abundance of 13C in marine organic matter and isotopic fractionation in the global biogeochemical cycle of carbon during the past 800 Ma, 1999.

Heijnen, M. S., Clare, M. A., Cartigny, M. J. B., Talling, P. J., Hage, S., Pope, E. L., Bailey, L., Sumner, E., Lintern, D. G., Stacey, C., Parsons, D. R., Simmons, S. M., Chen, Y., Hubbard, S. M., Eggenhuisen, J. T., Kane, I., and Hughes Clarke, J. E.: Fill, flush or shuffle: How is sediment carried through submarine channels to build lobes?, Earth and Planetary Science Letters, 584, 10.1016/j.epsl.2022.117481, 2022.

Hemingway, J. D., Schefuß, E., Dinga, B. J., Pryer, H., and Galy, V. V.: Multiple plant-wax compounds record differential sources and ecosystem structure in large river catchments, Geochimica et Cosmochimica Acta, 184, 20-40, 10.1016/j.gca.2016.04.003, 2016.

Hijmans, R. J., Cameron, S. E., Parra, J. L., Jones, P. G., and Jarvis, A.: Very high resolution interpolated climate surfaces for global land areas, International Journal of Climatology, 25, 1965-1978, 10.1002/joc.1276, 2005.
Hilton, R. G. and West, A. J.: Mountains, erosion and the carbon cycle, Nature Reviews Earth & Environment, 1, 284-299, 10.1038/s43017-020-0058-6, 2020.

Hilton, R. G., Galy, A., and Hovius, N.: Riverine particulate organic carbon from an active mountain belt: Importance of landslides, Global Biogeochemical Cycles, 22, 10.1029/2006gb002905, 2008.

Hilton, R. G., Galy, A., Hovius, N., Horng, M.-J., and Chen, H.: Efficient transport of fossil organic carbon to the ocean by steep mountain rivers: An orogenic carbon sequestration mechanism, Geology, 39, 71-74, 10.1130/g31352.1, 2011.

Hilton, R. G., Galy, A., Hovius, N., Kao, S.-J., Horng, M.-J., and Chen, H.: Climatic and geomorphic controls on the erosion of terrestrial biomass from subtropical mountain forest, Global Biogeochemical Cycles, 26, 10.1029/2012gb004314, 2012.

Hoffmann, B., Feakins, S. J., Bookhagen, B., Olen, S. M., Adhikari, D. P., Mainali, J., and Sachse, D.: Climatic and geomorphic drivers of plant organic matter transport in the Arun River, E Nepal, Earth and Planetary Science Letters, 452, 104-114, 10.1016/j.epsl.2016.07.008, 2016.

Hoover, T. M., Marczak, L. B., Richardson, J. S., and Yonemitsu, N.: Transport and settlement of organic matter in small streams, Freshwater Biology, 55, 436-449, 10.1111/j.1365-2427.2009.02292.x, 2010.

Hou, J., D'Andrea, W. J., and Huang, Y.: Can sedimentary leaf waxes record D/H ratios of continental precipitation? Field, model, and experimental assessments, Geochimica et Cosmochimica Acta, 72, 3503-3517, 10.1016/j.gca.2008.04.030, 2008.

Huang, Y., Clemens, S. C., Liu, W., Wang, Y., and Prell, W. L.: Large-scale hydrological change drove the late Miocene C4 plant expansion in the Himalayan foreland and Arabian Peninsula, Geology, 35, 10.1130/g23666a.1, 2007.

Iroumé, A., Ruiz-Villanueva, V., and Salas-Coliboro, S.: Fluvial transport of coarse particulate organic matter in a coastal mountain stream of a rainy-temperate evergreen broadleaf forest in southern Chile, Earth Surface Processes and Landforms, 45, 3216-3230, 10.1002/esp.4961, 2020.

Kao, S. J., Hilton, R. G., Selvaraj, K., Dai, M., Zehetner, F., Huang, J. C., Hsu, S. C., Sparkes, R., Liu, J. T., KC Denmark A/S: Helley-Smith Sampler: https://www.kc-denmark.dk/products/sediment-trap-station/helley-smith-sampler.aspx, last access: 20.09.2023.

Lee, T. Y., Yang, J. Y. T., Galy, A., Xu, X., and Hovius, N.: Preservation of terrestrial organic carbon in marine sediments offshore Taiwan: mountain building and atmospheric carbon dioxide sequestration, Earth Surface Dynamics, 2, 127-139, 10.5194/esurf-2-127-2014, 2014.

875     Lee, H., Galy, V., Feng, X., Ponton, C., Galy, A., France-Lanord, C., and Feakins, S. J.: Sustained wood burial in the Bengal Fan over the last 19 My, Proc Natl Acad Sci U S A, 116, 22518-22525, 10.1073/pnas.1913714116, 2019.

        Liu, J. T., Kao, S. J., Huh, C. A., and Hung, C. C.: Gravity flows associated with flood events and carbon burial:
880     Taiwan as instructional source area, Ann Rev Mar Sci, 5, 47-68, 10.1146/annurev-marine-121211-172307, 2013.
        Liu, Z., Zhao, Y., Colin, C., Stattegger, K., Wiesner, M. G., Huh, C.-A., Zhang, Y., Li, X., Sompongchaiyakul, P., You, C.-F., Huang, C.-Y., Liu, J. T., Siringan, F. P., Le, K. P., Sathiamurthy, E., Hantoro, W. S., Liu, J., Tuo, S., Zhao, S., Zhou, S., He, Z., Wang, Y., Bunsomboonsakul, S., and Li, Y.: Source-to-sink transport processes of fluvial sediments in the South China Sea, Earth-Science Reviews, 153, 238-273,
885     10.1016/j.earscirev.2015.08.005, 2016.

        McArthur, A. D., Kneller, B. C., Wakefield, M. I., Souza, P. A., and Kuchle, J.: Palynofacies classification of the depositional elements of confined turbidite systems: Examples from the Gres d'Annot, SE France, Marine and Petroleum Geology, 77, 1254-1273, 10.1016/j.marpetgeo.2016.08.020, 2016.
890
        Merten, E. C., Vaz, P. G., Decker-Fritz, J. A., Finlay, J. C., and Stefan, H. G.: Relative importance of breakage and decay as processes depleting large wood from streams, Geomorphology, 190, 40-47, 10.1016/j.geomorph.2013.02.006, 2013.

895     McGlue, M. M., Smith, P. H., Zani, H., Silva, A., Carrapa, B., Cohen, A. S., and Pepper, M. B.: An Integrated Sedimentary Systems Analysis of the Rio Bermejo (Argentina): Megafan Character in the Overfilled Southern Chaco Foreland Basin, J Sediment Res, 86, 1359-1377, 10.2110/jsr.2016.82, 2016.

        Nichols, G. J., Cripps, J. A., Collinson, M. E., and Scott, A. C.: Experiments in waterlogging and sedimentology
900     of charcoal: results and implications, Palaeogeography, Palaeoclimatology, Palaeoecology, 164, 43–56, https://doi.org/10.1016/S0031-0182(00)00174-7, 2000.

        Nieto-Moreno, V., Rohrmann, A., van der Meer, M. T. J., Sinninghe Damsté, J. S., Sachse, D., Tofelde, S., Niedermeyer, E. M., Strecker, M. R., and Mulch, A.: Elevation-dependent changes in n -alkane δ D and soil
905     GDGTs across the South Central Andes, Earth and Planetary Science Letters, 453, 234-242, 10.1016/j.epsl.2016.07.049, 2016.

        Parsons, D. R., Jackson, P. R., Czuba, J. A., Engel, F. L., Rhoads, B. L., Oberg, K. A., Best, J. L., Mueller, D. S., Johnson, K. K., and Riley, J. D.: Velocity Mapping Toolbox (VMT): a processing and visualization suite for
910     moving-vessel ADCP measurements, Earth Surface Processes and Landforms, 38, 1244-1260, 10.1002/esp.3367, 2013.

        Ponton, C., West, A. J., Feakins, S. J., and Galy, V.: Leaf wax biomarkers in transit record river catchment composition, Geophysical Research Letters, 41, 6420-6427, 10.1002/2014gl061328, 2014.
915
        Powell, R. L., Zoo, E.-H., and Still, C. J.: Vegetation and soil carbon-13 isoscapes for South America integrating remote sensing and ecosystem isotope measurements, Ecosphere, 3(11).109, https://doi.org/10.1890/ES12-00162.1, 2012.

920     Rach, O., Hadeen, X., and Sachse, D.: An automated solid phase extraction procedure for lipid biomarker purification and stable isotope analysis, Organic Geochemistry, 142, 10.1016/j.orggeochem.2020.103995, 2020.

        Reid, I., Laronne, J. B., and Powell, D. M.: Flash-flood and bedload dynamics of desert gravel-bed streams, Hydrological Processes, 12, 543-557, https://doi.org/10.1002 (SICI)1099-1085(19980330)12:4<543::AID-
925     HYP593>3.0.CO;2-C, 1998.

        Repasch, M., Scheingross, J. S., Cook, K. L., Sachse, D., Dosch, S., Orfeo, O., and Hovius, N.: Lithospheric Flexure Controls on Geomorphology, Hydrology, and River Chemistry in the Andean Foreland Basin, AGU Advances, 4, e2023AV000924, https://doi.org/10.1029/2023AV000924, 2023.
930
        Repasch, M., Scheingross, J. S., Hovius, N., Vieth-Hillebrand, A., Mueller, C. W., Höschen, C., Szupiany, R. N., and Sachse, D.: River Organic Carbon Fluxes Modulated by Hydrodynamic Sorting of Particulate Organic Matter, Geophysical Research Letters, 49, 10.1029/2021gl096343, 2022.

935    Repasch, M., Wittmann, H., Scheingross, J. S., Sachse, D., Szupiany, R., Orfeo, O., Fuchs, M., and Hovius, N.:
Sediment Transit Time and Floodplain Storage Dynamics in Alluvial Rivers Revealed by Meteoric10Be, Journal
of Geophysical Research: Earth Surface, 125, 10.1029/2019jf005419, 2020.

Rickenmann, D.: Variability of Bed Load Transport During Six Summers of Continuous Measurements in Two
940    Austrian Mountain Streams (Fischbach and Ruetz), Water Resources Research, 54, 107-131,
https://doi.org/10.1002/2017WR021376, 2018.

Rohrmann, A., Strecker, M. R., Bookhagen, B., Mulch, A., Sachse, D., Pingel, H., Alonso, R. N., Schildgen, T.
F., and Montero, C.: Can stable isotopes ride out the storms? The role of convection for water isotopes in
945    models, records, and paleoaltimetry studies in the central Andes, Earth and Planetary Science Letters, 407, 187-
195, 10.1016/j.epsl.2014.09.021, 2014.

Ruiz-Villanueva, V., Mazzorana, B., Bladé, E., Bürkli, L., Iribarren-Anacona, P., Mao, L., Nakamura, F.,
Ravazzolo, D., Rickenmann, D., Sanz-Ramos, M., Stoffel, M., and Wohl, E.: Characterization of wood-laden
950    flows in rivers, Earth Surface Processes and Landforms, 44, 1694-1709, 10.1002/esp.4603, 2019.

Sachse, D., Radke, J., and Gleixner, G.: Hydrogen isotope ratios of recent lacustrine sedimentary n-alkanes
record modern climate variability, Geochimica et Cosmochimica Acta, 68, 4877-4889,
10.1016/j.gca.2004.06.004, 2004.
955
Sachse, D., Billault, I., Bowen, G. J., Chikaraishi, Y., Dawson, T. E., Feakins, S. J., Freeman, K. H., Magill, C.
R., McInerney, F. A., Meer, M. T. J. v. d., Polissar, P., Robins, R. J., Sachs, J. P., Schmidt, H.-L., Sessions, A. L.,
White, J. W. C., West, J. B., and Kahmen, A.: Molecular Paleohydrology: Interpreting the Hydrogen-Isotopic
Composition of Lipid Biomarkers from Photosynthesizing Organisms, Annual Review of Earth and Planetary
960    Sciences, 40, 221-249, 10.1146/annurev-earth-042711-105535, 2012.

Sambrook Smith, G. H., Best, J. L., Leroy, J. Z., Orfeo, O., and Baas, J.: The alluvial architecture of a suspended
sediment dominated meandering river: the Río Bermejo, Argentina, Sedimentology, 63, 1187-1208,
10.1111/sed.12256, 2016.
965
Schefuss, E., Schouten, S., and Schneider, R. R.: Climatic controls on central African hydrology during the past
20,000 years, Nature, 437, 1003-1006, 10.1038/nature03945, 2005.

Scheingross, J. S., Hovius, N., Dellinger, M., Hilton, R. G., Repasch, M., Sachse, D., Gröcke, D. R., Vieth-
970    Hillebrand, A., and Turowski, J. M.: Preservation of organic carbon during active fluvial transport and particle
abrasion, Geology, 47, 958-962, 10.1130/g46442.1, 2019.

Scheingross, J. S., Repasch, M. N., Hovius, N., Sachse, D., Lupker, M., Fuchs, M., Halevy, I., Gröcke, D. R.,
Golombek, N. Y., Haghipour, N., Eglinton, T. I., Orfeo, O., and Schleicher, A. M.: The fate of fluvially-
975    deposited organic carbon during transient floodplain storage, Earth and Planetary Science Letters, 561,
10.1016/j.epsl.2021.116822, 2021.

Schlünz, B. and Schneider, R. R.: Transport of terrestrial organic carbon to the oceans by rivers: re-estimating
flux- and burial rates, International Journal of Earth Sciences, 88, 599-606, 10.1007/s005310050290, 2000.
980    Schwab, M. S., Hilton, R. G., Haghipour, N., Baronas, J. J., and Eglinton, T. I.: Vegetal Undercurrents—
Obscured Riverine Dynamics of Plant Debris, Journal of Geophysical Research: Biogeosciences, 127,
10.1029/2021jg006726, 2022.

Selva, E. C., Couto, E. G., Johnson, M. S., and Lehmann, J.: Litterfall production and fluvial export in
985    headwater catchments of the southern Amazon, Journal of Tropical Ecology, 23, 329-335,
10.1017/s0266467406003956, 2007.

Seo, J. I., Nakamura, F., Nakano, D., Ichiyanagi, H., and Chun, K. W.: Factors controlling the fluvial export of
large woody debris, and its contribution to organic carbon budgets at watershed scales, Water Resources
990    Research, 44, 10.1029/2007wr006453, 2008.

Silva, L. C. R., Giorgis, M. A., Anand, M., Enrico, L., Pérez-Harguindeguy, N., Falczuk, V., Tieszen, L. L., and Cabido, M.: Evidence of shift in C4 species range in central Argentina during the late Holocene, Plant and Soil, 349, 261-279, 10.1007/s11104-011-0868-x, 2011.

995

Smith, J. A., Mazumder, D., Suthers, I. M., Taylor, M. D., and Bowen, G.: To fit or not to fit: evaluating stable isotope mixing models using simulated mixing polygons, Methods in Ecology and Evolution, 4, 612-618, 10.1111/2041-210x.12048, 2013a.

1000    Smith, J. C., Galy, A., Hovius, N., Tye, A. M., Turowski, J. M., and Schleppi, P.: Runoff-driven export of particulate organic carbon from soil in temperate forested uplands, Earth and Planetary Science Letters, 365, 198-208, 10.1016/j.epsl.2013.01.027, 2013b.

Spacesystems, N. M. A. J. and Team, U. S. J. A. S.: ASTER Global Digital Elevation Model NetCDF V003,
1005    NASA EOSDIS Land Processes DAAC, https://doi.org/10.5067/MEaSUREs/NASADEM/NASADEM_NC.001, 2019.

Sparkes, R. B., Lin, I.-T., Hovius, N., Galy, A., Liu, J. T., Xu, X., and Yang, R.: Redistribution of multi-phase particulate organic carbon in a marine shelf and canyon system during an exceptional river flood: Effects of
1010    Typhoon Morakot on the Gaoping River–Canyon system, Marine Geology, 363, 191-201, 10.1016/j.margeo.2015.02.013, 2015.

Stallard, R. F.: Terrestrial sedimentation and the carbon cycle: Coupling weathering and erosion to carbon burial, Global Biogeochemical Cycles, 12, 231-257, 10.1029/98gb00741, 1998.

1015

Stewart, M. K. and Taylor, C. B.: Environmental isotopes in New Zealand hydrology ; 1 Introduction The role of oxygen-18, deuterium, and tritium in hydrology, New Zealand journal of science, 295-311, 1981.

Thomas, C. L., Jansen, B., van Loon, E. E., and Wiesenberg, G. L. B.: Transformation of n-alkanes from plant to
1020    soil: a review, Soil, 7, 785-809, 10.5194/soil-7-785-2021, 2021.

Turowski, J. M., Hilton, R. G., and Sparkes, R.: Decadal carbon discharge by a mountain stream is dominated by coarse organic matter, Geology, 44, 27-30, 10.1130/g37192.1, 2016.

1025    Turowski, J. M., Badoux, A., Bunte, K., Rickli, C., Federspiel, N., and Jochner, M.: The mass distribution of coarse particulate organic matter exported from an Alpine headwater stream, Earth Surface Dynamics, 1, 1-11, 10.5194/esurf-1-1-2013, 2013.

Tyson, R. V. and Follows, B.: Palynofacies prediction of distance from sediment source- A case study from the
1030    Upper Cretaceous of the Pyrenees, Geology, 28, 569–571, 2000.

Walker, C. D. and Richardson, S. B.: The use of stable isotopes of water in characterising the source of water in vegetation, Chemical Geology: Isotope Geoscience section, 94, 145-158, https://doi.org/10.1016/0168-9622(91)90007-J, 1991.

1035
West, A. J., Lin, C. W., Lin, T. C., Hilton, R. G., Liu, S. H., Chang, C. T., Lin, K. C., Galy, A., Sparkes, R. B., and Hovius, N.: Mobilization and transport of coarse woody debris to the oceans triggered by an extreme tropical storm, Limnology and Oceanography, 56, 77-85, 10.4319/lo.2011.56.1.0077, 2011.

1040    Wohl, E., Ogden, F. L., and Goode, J.: Episodic wood loading in a mountainous neotropical watershed, Geomorphology, 111, 149-159, 10.1016/j.geomorph.2009.04.013, 2009.

Wohl, E., Kramer, N., Ruiz-Villanueva, V., Scott, D. N., Comiti, F., Gurnell, A. M., Piegay, H., Lininger, K. B., Jaeger, K. L., Walters, D. M., and Fausch, K. D.: The Natural Wood Regime in Rivers, BioScience, 69, 259-273,
1045    10.1093/biosci/biz013, 2019.

Yager, E. M., Turowski, J. M., Rickenmann, D., and McArdell, B. W.: Sediment supply, grain protrusion, and bedload transport in mountain streams, Geophysical Research Letters, 39, n/a-n/a, 10.1029/2012gl051654, 2012.

1050